Solid–Electrolyte Interphase at Positive Electrodes in High-Energy Li-Ion Batteries: Current Understanding and Analytical Tools

Giorgia Zampardi*[a, b] and Fabio La Mantia*[a]

Batteries & Supercaps

Reviews
doi.org/10.1002/batt.201900177

**Chemistry
Europe**

European Chemical
Societies Publishing
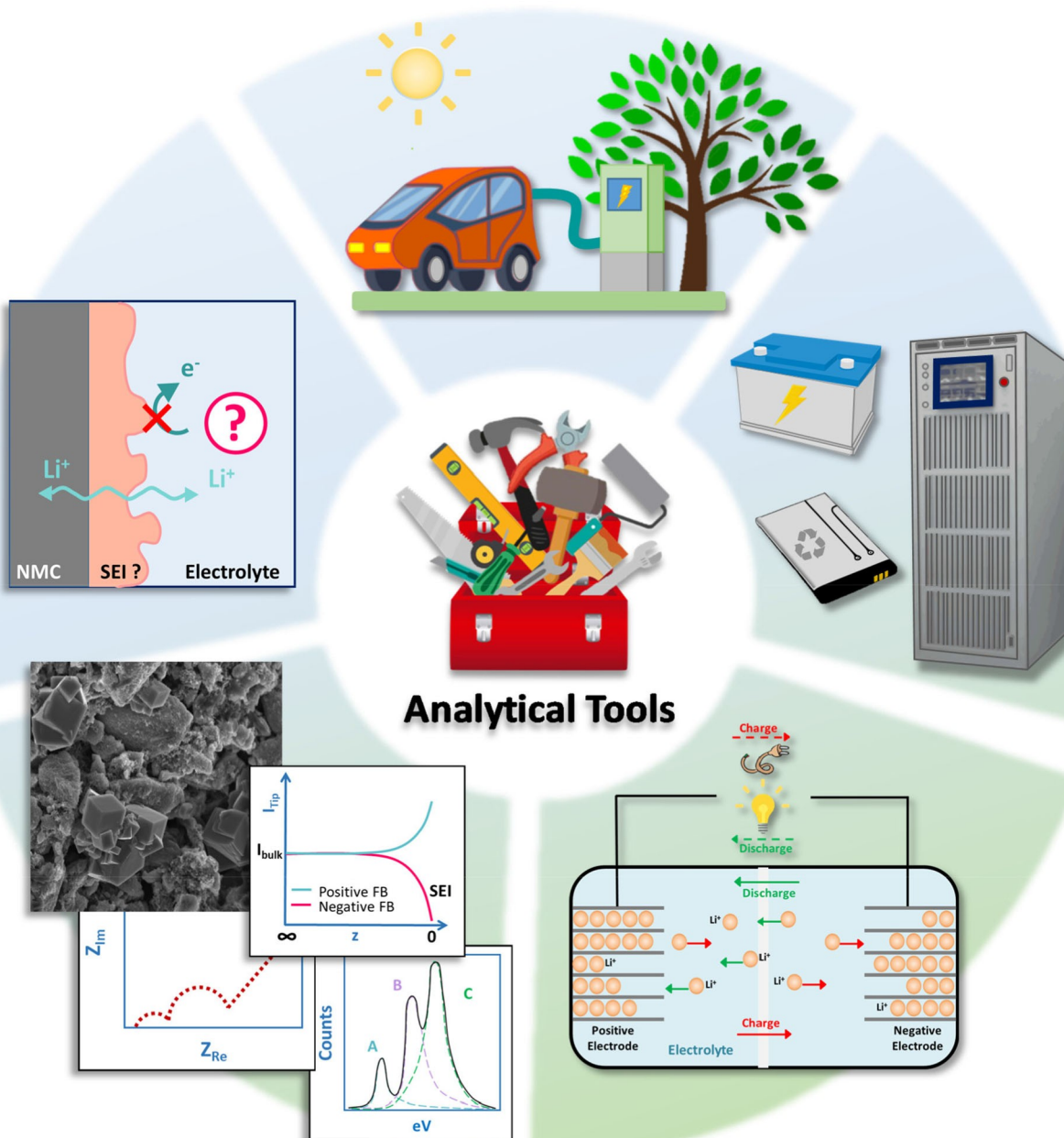
Abstract: The operating potentials of the Li-ion batteries active materials usually exceed the stability window of the electrolyte, leading to its irreversible reduction or oxidation. Often, as an effect of these side reactions, a surface layer is deposited onto the electrodes' materials. These surface layers play a pivotal role on the battery performance, rate capability, irreversible charge losses, and safety. Despite their importance, such interphases are difficult to analyse because of their small thickness and sensitive chemical composition. With this review, the authors intend to describe the already established analytical tools for the analysis of the interphase layers formed at the electrodes' surface in Li-ion batteries, together with the novel, unconventional ones under current development, focusing on the strengths and weak points of each technique. Particular attention will be given to the surface layers formed onto the positive electrodes through a summary of their current understanding. This is of main importance since understanding the interphase at the positive electrode side could enable the next generation of high energy Li-ion batteries.

1. Introduction and Scope of the Review

1.1. Solid-electrolyte Interphase: The Paradigm

In order to reach high operating voltage, Li-ion batteries are conventionally based on aprotic organic electrolytes, because of their broad stability window (more than 3 V compared to the c.a. 2 V of water).[1–2] Nevertheless, several active materials used in today's Li-ion batteries operate outside the thermodynamic stability window of the non-aqueous electrolytes. These conditions cause an irreversible decomposition of the electrolyte, often resulting in the formation of a more or less stable surface layer, which is interposed between the electrode and the electrolyte.

This surface layer was observed for the first time on metallic lithium during the irreversible reduction of the electrolyte, which occurs upon direct contact between the metallic lithium and the electrolyte, and it was called "solid-electrolyte interphase" (SEI) because of its 3D structure.[3–4] The SEI has some very peculiar physicochemical characteristics: it is an electronic insulator and a Li^+ conductor, thus by definition it can be considered as an *electrolyte.* In this way, any further irreversible decomposition of the organic electrolyte is prevented, or at least is slowed down, whilst Li ions can still take part to the electrode's reactions.

Researchers soon understood the pivotal importance that the SEI had on the overall battery system, since its presence stabilised the graphite negative electrodes, thus enabling the commercialisation of the Li-ion technology.[5–7] In particular, graphite can intercalate Li^+ in a potential range between 0.3 V and 0.05 V vs. Li/Li^+ (c.a. −2.75 V and −3 V vs. SHE, respectively), in which the electrolyte undergoes a severe irreversible reduction. Since the lithium ions enter within the graphite structure with at least part of their solvation shell, solvent molecules are co-intercalated together with Li^+. At such low cathodic potentials, the solvent molecules inside the graphite structure are irreversibly reduced, resulting in the formation of gaseous products, which destroy the graphite matrix (exfoliation).[3,8–9] This deleterious phenomenon can be prevented when a stable SEI is formed onto the graphite electrode, allowing a reversible Li^+ (de-)intercalation.[6]

The energy band model can well explain the thermodynamic reasons of the interphase formation, together with its role in a Li-ion battery.[10] To better understand the sketch of the energy levels of the interfaces of a Li-ion battery, let us focus on the system from a purely thermodynamic point of view.

A Li-ion battery can be described through a Galvani representation (Figure 1) consisting of several phases in contact: two solid electron conductive phases (α', α''), the electrodes (σ', σ''), and the ion conductive phase, the electrolyte (ε).

At open circuit conditions, the Li-ion cell is thermodynamically stable, thus all phases are at electrochemical equilibrium, and all the species (electrons or ions) existing in both the phases in contact are not subjected to any net transport from a phase to another. Under this condition, the following equilibria between the different phases in contact can be derived [Eqs. (1)–(4)]:

$$\text{Phases } \alpha'/\sigma' : \quad \tilde{\mu}_e^{\alpha'} = \tilde{\mu}_e^{\sigma'} \tag{1}$$

$$\text{Phases } \sigma'/\varepsilon : \quad \mu_{Li}^{\sigma'} = \tilde{\mu}_e^{\sigma'} + \tilde{\mu}_{Li+}^{\varepsilon} \tag{2}$$

$$\text{Phases } \varepsilon/\sigma'' : \quad \mu_{Li}^{\sigma''} = \tilde{\mu}_e^{\sigma''} + \tilde{\mu}_{Li+}^{\varepsilon} \tag{3}$$

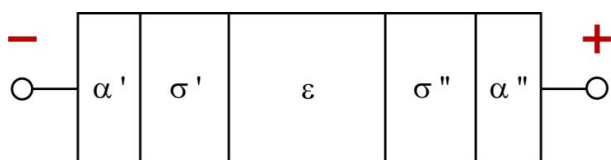$$\text{Phases } \sigma''/\alpha'' : \quad \tilde{\mu}_e^{\alpha''} = \tilde{\mu}_e^{\sigma''} \tag{4}$$

The open circuit potential V_{OC} is the potential difference measured at the two external contacts α' and α'', which corresponds, considering Equations (1) and (4), to the difference in the electrochemical potentials of the electrons in the solid phases (cathode and anode) [Eq. (5)]:

[a] Dr. G. Zampardi, Prof. Dr. F. La Mantia
Universität Bremen
Energiespeicher- und Energiewandlersysteme
Bibliothekstrasse 1, 28359 Bremen, Germany
E-mail: zampardi@uni-bremen.de
lamantia@uni-bremen.de

[b] Dr. G. Zampardi
Department of Chemistry
Physical and Theoretical Chemistry Laboratory
University of Oxford
South Parks Road, OX1 3QZ Oxford, United Kingdom

Batteries & Supercaps

Reviews
doi.org/10.1002/batt.201900177

Chemistry Europe
European Chemical
Societies Publishing

Figure 1. Galvani representation of a Li-ion battery, in which each Greek letter represents a phase. In particular: α' is the external (copper) metallic contact of the negative electrode; σ' is the negative electrode; ε the electrolyte, σ'' the positive electrode, and α'' the external (copper) metallic contact of the positive electrode. It is worth pointing out that the external contacts (α' and α'') do not have to be confused with the electrodes current collectors.

$$V_{OC} = V^{\alpha''} - V^{\alpha'} = \frac{\tilde{\mu}_e^{\alpha''} - \tilde{\mu}_e^{\alpha'}}{F} = \frac{\tilde{\mu}_e^{\sigma''} - \tilde{\mu}_e^{\sigma'}}{F} \qquad (5)$$

By subtracting Equation (3) from equation (2), it can be concluded that the open circuit potential of a Li-ion battery depends on the difference of the chemical potential of the lithium in the two solid phases [Eq. (6)]:

$$\mu_{Li}^{\sigma''} - \mu_{Li}^{\sigma'} = \tilde{\mu}_e^{\sigma''} - \tilde{\mu}_e^{\sigma'} = F \, V_{OC} \qquad (6)$$

In the energy diagram this can be translated at equilibrium (i.e., open circuit conditions) in a difference of the Fermi levels of the electrodes, as shown in Figure 2a. In this scheme, the stability window of the electrolyte (i.e. the energy gap, E_g) is represented by the difference in energy of its lowest unoccupied molecular orbital (LUMO) and its highest occupied molecular orbital (HOMO). The Fermi levels of the positive and the negative battery electrodes (which correspond to the cathode and the anode only during the discharge of the battery) must lay within the stability window of the electrolyte in order to ensure the thermodynamic stability of the battery at open circuit.

Upon charge (Figure 2b), the electrons flow in the negative electrode, thus increasing its Fermi level (E_F') which is now above the LUMO level of the solution, inducing the (irreversible) reduction of the electrolyte. At the same time upon charge, electrons leave the positive electrode, thus lowering its Fermi level (E_F''), which is now below the HOMO level of the solution, inducing in this case the (irreversible) oxidation of the electrolyte. The irreversible reductive and oxidative decomposition of the electrolyte can only be prevented kinetically, if a protective "passivating-like" layer is formed, which acts as a barrier against the electron transfer between the electrodes and the electrolyte (Figure 2c).

The energy band model clearly shows that the *electronically insulating character* is one of the most important characteristics of the interphase layers, since it prevents the electrolyte decomposition. Of course, an ideal interphase should have other very important properties, such as:

- high *ionic conductivity* and *selectivity towards Li ions*, in order to ensure the battery operation in high power regime;
- high *thermal stability* in order to allow the operation of the battery at high temperature and/or in spite of thermal oscillations occurring during the battery operations;
- high *mechanical stability* against the volume expansion/shrinkage during the Li$^+$ (de-)insertion processes;
- low *charge consumption*, in order to avoid a low coulombic efficiency of the overall battery system.

Several models have been proposed during the years to describe the structure of the SEI formed on carbonaceous materials upon the irreversible reduction of the electrolytes, some of which are schematically represented in Figure 3. Besenhard and co-workers proposed that a portion of the SEI could penetrate into the graphite layered structure, with consequent partial inclusion of solvent molecules.[11] The solid polymer layer model (Figure 3a) considers the SEI as a dispersion of solid inorganic compounds in a polymeric/oligomeric matrix.[12] The mosaic model (Figure 3b) suggests that the SEI could be formed as an agglomeration of several micro-phases, and assumes that the deposition of the organic and the inorganic compounds occurs simultaneously.[13–14] In the compact stratified layer model instead (Figure 3c), the SEI is seen as constituted by two sub-layers, a rigid one mainly inorganic, which lies closer to the electrode surface, and a soft one mainly organic/polymeric, which lays closer to the electrolyte.[12,15]

Following the compact stratified model, recently a membrane model has been proposed.[16] This model assumes that the inner inorganic-based layer of the SEI is not homogeneous, but rather contains active sites allowing the electron-transfer up to a certain extent. Moreover, the organic-based outer layer of the SEI in this case is supposed to behave like a membrane, *selectively* rather than sterically allowing or hindering the transport of ions and/or molecules.[16]
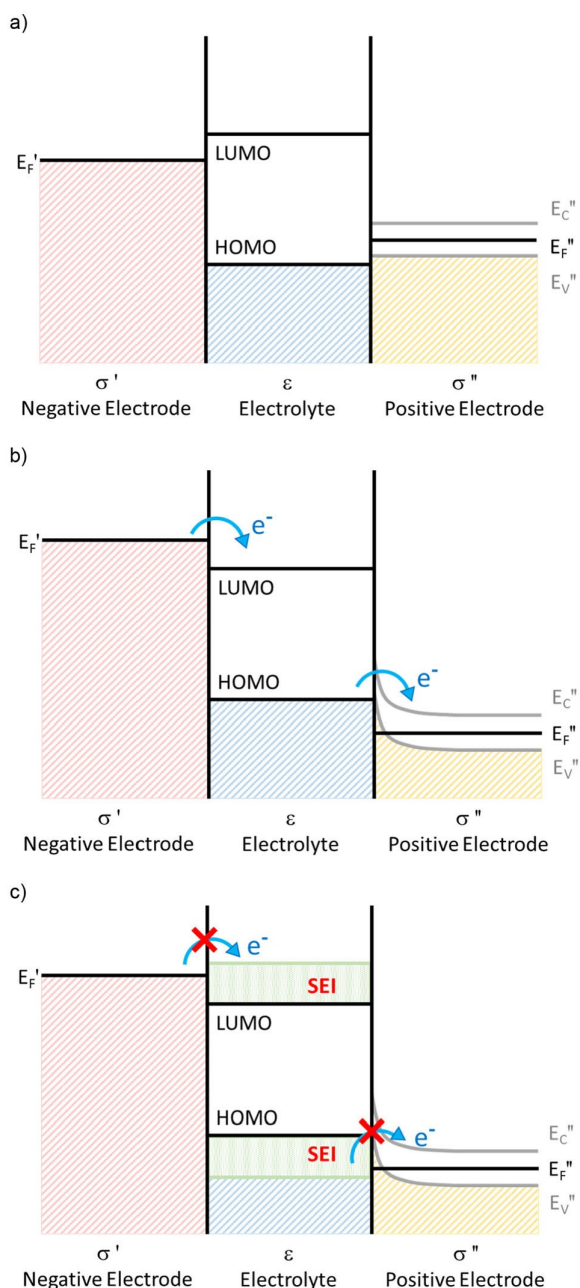
Although an ideal SEI is supposed to block completely the electron transfer and concomitantly to allow only the transport of Li$^+$ cations, the real situation is different. Even excluding the aging of the electrode materials *per se*, at least some of the irreversible reactions occurring during the cycle life of a Li-ion battery involve

Giorgia Zampardi received her Ph.D. in electrochemistry in 2015 from the Ruhr-University Bochum. She has been post-doctoral fellow at the University of Oxford, and she is currently postdoctoral researcher at the University of Bremen. Her research interests cover Li-ion batteries, aqueous metal-ion batteries, and novel electro-analytical methods for the study of surface and bulk phenomena in energy storage and conversion systems.
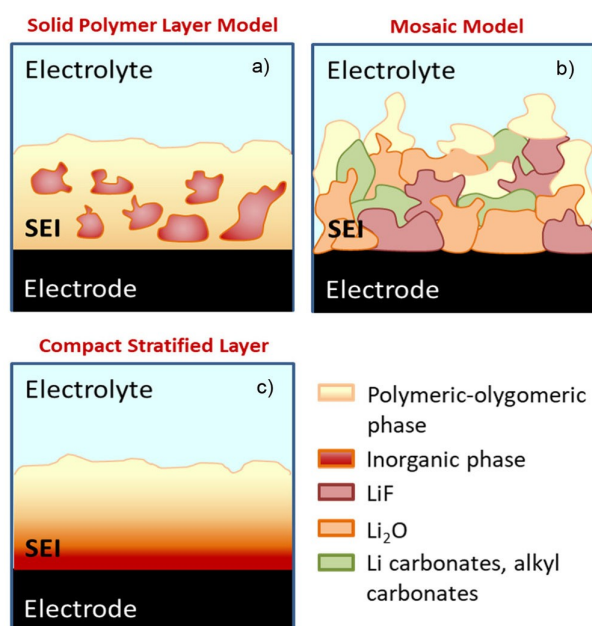
Fabio La Mantia received his Ph.D. in electrochemistry in 2008 from the ETH Zürich. He was a post-doctoral fellow at Stanford University, and he is currently full professor at the University of Bremen. His research interests ranges from Li-ion batteries and aqueous metal-ion batteries, to dynamic impedance spectroscopy and frequency response analysis.

Batteries & Supercaps

Reviews
doi.org/10.1002/batt.201900177

**Chemistry
Europe**
European Chemical
Societies Publishing

Figure 2. Schematic representation of the energy levels of a lithium ion battery, where the negative and the positive electrode phases, σ′ and σ″ respectively, are in contact with the electrolyte (phase ε): a) at open circuit conditions; b) upon charge; c) upon charge after the formation of the interphase layers on the two electrodes. In this scheme, the negative electrode is represented as a metal, whilst the positive electrode as a semiconductor, with a valence and a conduction band (whose energy levels are $E_V″$ and $E_C″$, respectively).

Figure 3. Schematic representation of the structure of the SEI proposed through: a) the solid polymer layer model, b) the mosaic model, and c) the compact stratified layer model.

a residue reduction of solvents molecules and other species.[7,16–17] Such residue irreversible reduction may be caused by: (I) a non-completely electronic insulating nature of the interphase, (II) non-homogeneous thickness of the SEI, allowing in some portions a direct electron tunnelling; (III) cracks in the interphasial layer, exposing electronically conductive surface to the electrolytes, (IV)

permeability of the interphase to chemical species (e.g. solvent molecules, salt, etc.).

The permeability of the SEI towards chemical species has a dual nature: on the one side, it is desirable that the SEI would completely block the through-film transport of species in order to avoid any further irreversible reaction involving the electrolyte constituents of the battery. On the other side, a certain through-film permeation degree is necessary for the correct functioning of the redox shuttles needed for the overcharge protection of the Li-ion cell. Ideally, the SEI should be permeable to the redox shuttle additives, but not permeable to the solvent molecules. In this respect, the permeation degree of the SEI towards some chemical species in general, and some redox shuttles in particular, can be studied through rotating (ring-)disk analysis mainly of glassy carbon electrodes and highly oriented pyrolytic graphite.[16,18–19] These studies demonstrated the blocking effect of the SEI towards the through-film transport of ferrocene and a more extensive permeation degree of 2,5-di-tert-butyl-1,4-dimethoxybenzene, making the latter better suited as additive for the battery overcharge protection.[19] Moreover, following the compact stratified layer model it has been suggested that of the two layers that are most likely composing the SEI, the compact one closer to the electrode surface may be formed by round-shaped particles, whilst the external one closer to the electrolyte side may be highly porous.[20] Here, the authors demonstrated that only the inner part of the SEI behaves as an electrolyte, allowing trough-film transport selectively for lithium, whilst the outer part is porous and non-selective. Recently, a detailed study on the permeation degree of a variety of substituted ferrocene molecules demonstrated that the through-film transport selectivity towards some species is chemical rather than steric.[16]

Batteries & Supercaps

Reviews
doi.org/10.1002/batt.201900177

Chemistry Europe
European Chemical
Societies Publishing

More attention should be paid to the study of the transport properties of chemical species (as solvent and other organic molecules) through the SEI, in view of gathering not only a better understanding of the structure and the physicochemical nature of the interphase, but also on the effectiveness of the redox shuttles employed for the battery overcharge protection.[16,21]

It is worth mentioning that, despite the fact that the SEI has been studied for many years, the mechanism of its formation, its exact structure and through-film transport properties are still unclear and under debate. This can be explained considering the high complexity of the several reactions involved in its formation, and because of the strong sensitivity of the SEI composition to the solvents, salts and additives present in the electrolyte, to the binders present in the electrode matrix, to contaminants like air and moisture, etc.[5–6,22]

In fact, despite the enormous importance of the SEI formed onto the negative electrodes, which controls the performance of the overall battery cell,[22–24] the reasons of the uncertainty regarding its formation mechanism, transport properties and structure are to be found in its sensitive chemical nature and, above all, lack of reliable *operando* tools.[17,22–23] Moreover, some characteristics and features attributed to the SEI are *often inferred rather than directly measured.* This results in a partial and unfortunately not comprehensive picture of the SEI characteristics and formation mechanism.

For more a more detailed and comprehensive discussion on the current understanding of the SEI formed onto the negative electrodes, we suggest the reader to refer to the following dedicated critical reviews: Refs. [6-7, 17].

1.2. Interphase on Positive Electrodes: The Veiled Dilemma

As long as Li-ion batteries were used only for portable electronic applications, most of the research efforts were directed towards the understanding of the surface layer formed on the negative electrodes (carbonaceous ones in particular) upon the irreversible reduction of the electrolytes, since it was found that a stable SEI dictates the cycle life and the safety of a Li-ion battery.[6–7,22–23,25–26] Moreover, the materials usually employed as positive electrodes (such as $LiFePO_4$, $LiCoO_2$, etc.) in the commercial Li-ion batteries for portable electronic applications have an operating potential below or slightly above the anodic thermodynamic stability window of the electrolytes.[7,27–28] Therefore, the anodic stability of the electrolyte was not a matter of primary concern.

However, the growing interest in electric powered vehicles pushed lately the development of Li-ion batteries towards higher energy densities, in terms of higher voltage of the cell. Therefore, materials operating at high anodic potentials are under current development,[29–31] opening up the question of the anodic stability of the electrolytes as well, as schematically depicted in Figure 4.

Understanding the properties of the surface layer between the positive electrode and the electrolyte is of practical importance since several factors such as the potential that can
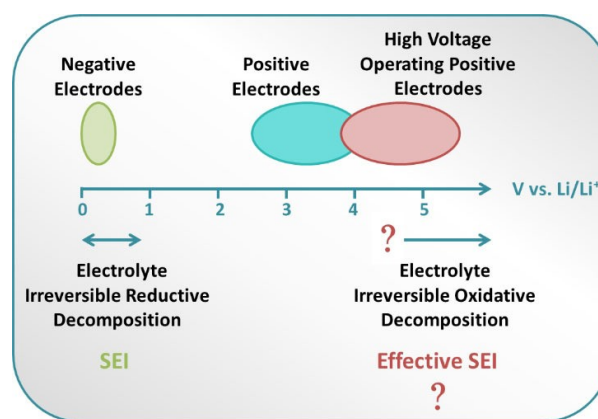
Figure 4. Simplified schematic representation of the operating potential range of the electrodes employed in Li-ion batteries, together with the instability potentials range of the electrolytes.

be reached during the battery cycling, and the overcharge margins that an electrolyte can provide depend on the nature of the interphase between electrode and electrolyte.[6–7,17]

Despite the ongoing debate on the nature and the characteristics of the positive electrode/electrolyte interphase, it is generally agreed that a surface layer is formed upon the irreversible oxidation of the electrolyte as well.[7,17,32–38] The existence of a surface layer on the positive electrode side has been reported for a variety of active materials, solvents, and lithium salts,[29,32–41] and in some cases independently of the synthesis route adopted for the active materials' preparation.[42]

Unfortunately, measuring the oxidation potentials of the electrolyte on the positive electrodes has been proved to be more challenging than on the negative electrode side, since some of the reactions are chemical, rather than electrochemical in nature.[34,36, 43] Moreover, several evidences point towards a catalytic influence of the material surface on the above-mentioned reactions, whose effect is not straightforwardly identified.[36–38,44]

Attempts to measure the anodic stability limit of the electrolytes have been made with the aid of non-active electrodes,[7,45–50] which however do not reflect the real situation when particulate active materials are employed.[49,51] On the other hand, the complex nature of the real, porous positive electrodes leads to ambiguous results of more difficult interpretation when conventional spectroscopic techniques (i.e. X-ray photoelectron spectroscopy, Fourier transform infra-red spectroscopy, etc.) are employed to study the surface layers.[7,36, 52] Further complications arise from the fact that a thin layer of native Li_2CO_3, one of the main products of the electrolyte irreversible oxidation,[32,35,53–55] already exists on the surface of transition metal oxides based on Mn, Ni and Co.[35,43,53,56–58] Moreover, such native Li_2CO_3 thin layer can spontaneously react with the electrolyte, acidic in nature due to the presence of fluorinated anion such as PF_6^-, BF_4^-, etc., leading to the formation of LiF, PO_xF_y species.[41,58–59] Other spontaneous chemical reactions proceeding via radical inter-mediate are suggested to occur at the positive electrode upon contact with the electrolyte and upon cycling the positive

Batteries & Supercaps

Reviews
doi.org/10.1002/batt.201900177

Chemistry Europe
European Chemical
Societies Publishing

electrode, involving the active material itself.[32,41,60] Such spontaneous chemical reactions further hinder the precise identification of the anodic stability limit of the electrolyte.

The composition and structure of the surface layer on the positive electrode side is also still unclear and under debate. It has been reported that such surface layer may be mainly constituted by polymeric/oligomeric species,[61] however inorganic components have been detected as well.[32,55,62–64] Interestingly, X-ray photoelectron spectroscopy studies suggested that the organic polymeric/oligomeric species composing the surface layer are formed independently of the active material composing the positive electrode, and their amount increases with increasing temperature.[32] On the contrary, the nature and amount of the inorganic species composing the surface layer have been found to be dependent on active material constituting the electrode.[32]

The physicochemical nature of the surface layer resulting from the oxidative electrolyte decomposition, remains still unclear and under debate within the scientific community. Aurbach et al. and Guyomard et al. initially inferred that such surface layer should have the same physicochemical characteristics as the one formed on graphite (i.e. electronically insulating and Li ion conducting).[35,39–40] Edström et al. called this surface layer solid permeable interphase (SPI)[32,55] referring to the permeability of such layer towards solvent and salt molecules, and suggested that its composition may be strongly dependent on the active material, in terms of the deposited organic and inorganic compounds. More recently, some evidences suggested that this surface layer might not be electronically insulating.[55,59,61,65] If the reason for that has to be found in the very small thickness of such surface layer, in the inhomogeneous distribution of its constituents, in its very physicochemical nature, or in a combination of them, remains still unclear and further investigation is needed.

It is worth considering that up to now no general agreement has been established within the scientific community regarding the physicochemical characteristics of the interphase formed at the positive electrodes. For this reason, different authors refer to such surface layer with a different terminology, such as "solid permeable interphase" (SPI),[32,55] "cathode–electrolyte interphase" (CEI),[42] or, as in the case of negative electrodes, "solid–electrolyte interphase" (SEI).[29,41] The fact that no unambiguous denomination has been given to such surface layer, can be directly related to the lack of a definite understanding of its role in the overall Li-ion cell.

The question that remains open, which thus requires further investigation, follows: *does this surface layer behave as a real electrolyte (electron insulator and ion conductor)?*

Considering that further experimental evidences are needed in order to understand the physicochemical nature of the surface layer formed upon the oxidative electrolyte decomposition, within this review we will refer to it as "surface layer", in order not to involuntarily suggest that such layer may have a similar physicochemical nature to the SEI.

1.3. Scope of the Review

As mentioned in the previous paragraphs, the investigation of the SEI in general, and of the surface layers formed upon the irreversible oxidation of the electrolyte in particular, poses numerous challenges. Some of such challenges are related to the intrinsic nature of the interphases (e.g. small thickness, similar constituents to the bulk material of the electrode, high chemical reactivity towards contaminants, etc.), introducing difficulties in the interphase detection and analysis. Other challenges arise from the tools employed for the interphase analysis themselves, since they are sometimes invasive, leading to unwanted changes in the physicochemical nature of the surface layers under investigation. Moreover, every analytical tool is able to determine some of the interphase properties, but is blind to others, resulting in a partial and unfortunately not comprehensive picture of the interphase characteristics.

For these reasons, and considering the high complexity of the processes involved in the interphase formation, in order to collect more clues about its nature, unconventional *in situ* analytical tools are under current development.[17] However, in order to gain a more comprehensive picture of the interphases of a Li-ion battery, not only novel *in situ* and *operando* tools have to be developed, but also a hyphenation of the several analysis tools is required.

In this review, the established techniques (Section 2) together with the promising unconventional analytical tools (Section 3) used for the interphase investigation in Li-ion batteries will be thoroughly discussed. The characteristics of the various techniques, together with their strengths and weaknesses, will be summarised in Table 1. Finally, the current understanding of the nature and the characteristics of the surface layers formed onto some high energy Li-ion batteries' active materials, promising for electromobility applications, and onto the inactive battery components will be described (Section 4).

2. Established Analytical Techniques for the Interphase Investigation in Li-Ion Batteries

2.1. Electron Microscopy

Imaging techniques, as scanning electron microscopy (SEM) and transmission electron microscopy (TEM) have always been extensively used in order to acquire information regarding the status of health, as well as the morphology changes of the surface of the lithium-ion battery electrodes during their cycle life.[66] For this reason, SEM and TEM have become routine analysis tools employed to visualise the surface morphological changes of the materials due to the SEI formation, and to estimate the SEI thickness.[66–68] During SEM analysis, a beam of accelerated electrons is used to image the surface of the sample, whilst with TEM the electron beam permeates the sample under analysis, allowing in this way the imaging of fine details of the sample's structure. Major advantages of the SEM employment for the study of the interphases in lithium-ion batteries lay in the fact that SEM

Batteries & Supercaps

Reviews
doi.org/10.1002/batt.201900177

**Chemistry Europe**
European Chemical
Societies Publishing

Table 1. Summary of the characteristics of the analytical tools employed for the interphase analysis in Li-ion batteries.

Analytical tool	Interphase analysis	Strength	Weakness
SEM, TEM	Morphology, thickness	Real-life electrodes analysis, interphase easy to visualise	*Ex situ*, invasive high energy beam, high vacuum, local analysis only
XPS	Composition	High precision, real-life composite electrodes analysis	*Ex situ*, invasive high energy beam, ultrahigh vacuum, difficult spectra interpretation
FTIR	Composition	*In situ*, non-invasive, quantitative	Low signal-to-noise ratio, difficult spectra interpretation, flat polished electrode analysis
DEMS	Gaseous products identification	*Operando*, *in situ*, quantitative, non-destructive, real-life electrodes analysis	Difficult cell design, gas evolution is not always correlated to an interphase formation
EIS	Overall electric resistance of the electrode	*In situ* and possibly *operando*, non-destructive	Extreme complexity (generally underestimated) of data acquisition and data interpretation
AFM	Morphology, growth, thickness, mechanical properties	*In situ*, *operando*, non-invasive	Thickness and mechanical properties estimation not always reliable, local analysis only, sometimes surface polished electrodes needed
SECM	Electronic character	*In situ*, *operando*, non-destructive, both local and average analysis possible, real-life electrode analysis	Not trivial cell design, limited cycles during the *operando* analysis, redox mediator needed, possible particle dragging during area mapping
Neutron-based techniques	Composition, structure, thickness	*In situ*, *operando*, non-destructive, high resolution	Limited instrument availability, difficult cell design, generally employed *ex situ*, flat surface electrode analysis only
Ellipsometry	Thickness, growth, density	Non-destructive, high accuracy, *in situ*	Generally applied *ex situ*, difficult cell design, needs reliable models for data interpretation, flat surface electrode analysis only
Fluorescence microscopy	Preferential reaction site visualisation, identification of species travelling between electrodes	*In situ*, high resolution	Mostly applied *ex situ*, only fluorescent species can be visualised, often unknown composition of the visualised species
EQCM	Growth, thickness, viscoelastic properties	*In situ*, *operando*, non-destructive, real-life electrodes analysis	Mass per charge ratio often does not reflect real stoichiometry, difficult setup design, reliable models needed to take into account the electrode porous structure
XAS	Composition, reaction intermediates	*In situ*, high selectivity and precision, real-life electrodes analysis possible	Generally applied *ex situ*, invasive high energy beam ad ultrahigh vacuum conditions needed when synchrotron used as beam source, difficult cell design, flat and thin polycrystalline samples preferred, not trivial interpretation of the collected data

is easy to use, and it provides a quick way of obtaining images of the morphology changes of the electrodes. Moreover, real, porous composite electrodes can be analysed through SEM, without needing the use of ideal materials with a flat-finished surface. Recently, a low energy SEM-based technique with extra high resolution has been developed, which provided local thickness imaging of the SEI thanks to the secondary electron contrast mechanism (Figure 5).[69] TEM analysis is routinely employed to visualise interphases and to estimate their thickness. The amorphous character of the interphase appears in strong contrast against the typical crystallinity of the particles of the active material on which it grew, resulting in an enhanced resolution of the SEI thickness.[17]

2.1.1. Limitations of electron microscopy

The biggest limitation in using electron microscopy to study the interphases in lithium-ion batteries is related to the intrinsic *ex situ* nature of the analysis. Therefore, a possible relaxation of the material, if analysed in metastable conditions, and a possible contamination with air and moisture during the transport of the sample from the glovebox to the microscope must be taken into account.[62,70–71] These may result in a change of the chemical and structural properties of the interphase.[62,66,70–71] Moreover, the high energy electron beam, together with the high vacuum conditions to which the electrode is exposed during the analysis, may promote a degradation of the organic species of the interphase and may produce artefacts, which therefore can lead to misleading conclusions.[66] Due to its invasive and *ex situ* character, electron microscopy analysis has to be carried out with a large number
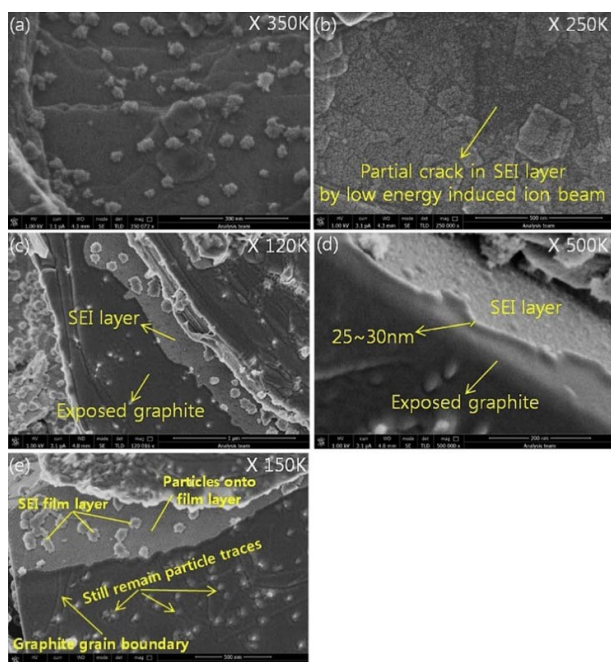
Figure 5. XHR-SEM images of SEI layer on graphite electrode for formation cell: a) before ion etching, b) after ion etching for 2 min, and c, d, e) after ion etching for 5 min. Reprinted with permission from Ref. [69] Copyright (2013) Elsevier.

of samples, in order to collect data that are representative of the overall electrode. Even in this case however, the question of how representative of the overall electrode such localised information is remains open.

A further problem arises regarding the applicability of such analysis to the interphase formed onto positive electrodes: in this case, it is much more difficult to visualise the surface layers formed on the positive electrode side through electron microscopy and to estimate correctly their thickness, since such surface layers are thinner than their counterparts formed in the negative electrode side.[32,41,59]

2.2. X-Ray Photoelectron Spectroscopy

The ability of analysing the constituents of a material surface, made X-rays photoelectron spectroscopy (XPS) one of the most widely used techniques to study the elements and the chemical species composing the SEI.

During XPS analysis, a high energy incident X-ray beam penetrates the material for several hundreds of nanometres and electrons are emitted from the core of the atoms present only on the surface of the sample (within the first few nanometres), because of their short inelastic mean free path.[72] The kinetic energy of the detected electrons is correlated with the binding energy of the level from which the electron is emitted. This allows identifying the elemental composition of the material's surface. All the elements present on the surface under analysis can be identified, with the exception of hydrogen and helium, if their concentration is above 0.1 at%.[6]

Moreover, information about the chemical surrounding of the element can be extracted as well (e.g. C−C, C−O, C=O, etc.) by evaluating the shifts in the binding energies.[6,72] For these reasons, the use of XPS has been proved to give valuable information about the identification of the inorganic and organic components present in the interphase layers.[6,52,70]

2.2.1. Limitations of XPS

XPS analysis of the surface layers in lithium-ion batteries is almost exclusively carried out *ex situ*, therefore careful attention must be paid during the handling of the sample, especially during its transportation from the Ar-filled glovebox to the vacuum chamber of the spectrometer. Most of the components of the surface layer of Li-ion battery electrodes suffer from dramatic sensitivity towards air, and this can lead to misinterpret the presence and the amount of some surface compounds like Li_2CO_3, Li_2O and LiF. As an example, it has been recently demonstrated that no Li_2CO_3 signal was present in the XPS spectra of the surface of cycled graphite electrodes when stored and transported in an in-house designed vessel hermetically sealed.[62,70] The signal of Li_2CO_3 that is often detected in the SEI formed on graphite is most probably due to the contamination of the samples with a small amount of air, which comes in contact with the electrode during the transport step from the glovebox to the XPS vacuum chamber.[70–71]
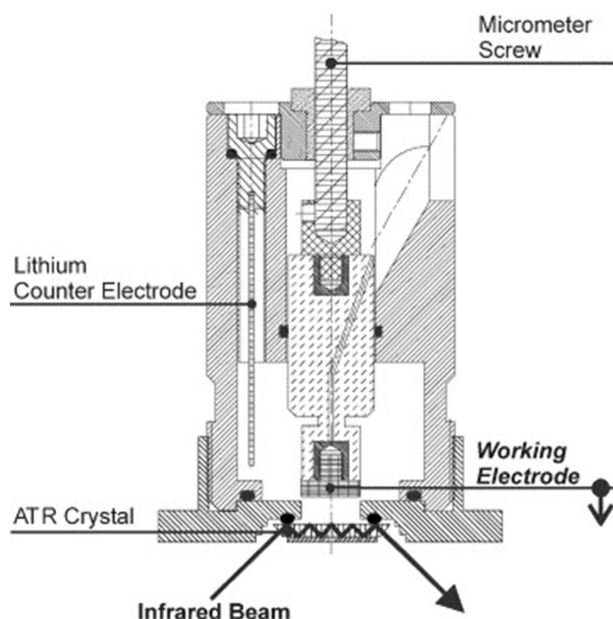
Moreover, the use of high energy photons may alter the composition of the surface of the electrodes, and the ultrahigh vacuum conditions needed for the operation of the system can damage or partially decompose the chemical species of the surface layer.[52] Furthermore, the estimation of the interphase thickness through XPS must be carefully considered, since undesired chemical reaction can be promoted by the sputtered ions.[6] Last but not the least, the interpretation of the XPS spectra is not straightforward, and it should be based on a solid knowledge of the systems and good reference values.[6]

The situation is further complicated when XPS is to be used for the analysis of the surface layers on positive electrodes in lithium-ion batteries. In this case, in fact, the identification and the quantification of the species present at the interface arising from the irreversible decomposition of the electrolyte become extremely difficult, since substrate and surface have the same elements, leading in this way to ambiguous results of more difficult interpretation.[6,52]

2.3. Fourier Transform Infrared Spectroscopy

As XPS, Fourier transform infrared spectroscopy (FTIR) is routinely employed to investigate the composition of the surface layers formed onto lithium-ion battery electrodes.[6,68,73–74] The working principle of FTIR is based on the characteristic bond vibrational energies. Therefore, FTIR can differentiate among diverse functional groups depending on their dipole moments.[6]

Batteries & Supercaps

Reviews
doi.org/10.1002/batt.201900177

Chemistry
Europe
European Chemical
Societies Publishing

Figure 6. The electrochemical cell for in situ infrared spectroscopy with the working electrode shown in the position back from the optical window. Reprinted with permission from Ref. [80]. Copyright (2005) Elsevier.

One of its main advantages lays in the fact that FTIR is a non-destructive method. In fact, the instrumental apparatus employs beams with low energy wavelengths in the micron range (100 μm–1 μm) to irradiate the sample under analysis, therefore no high energy rays or ultrahigh vacuum conditions are required. In this way, any alteration of the components of the surface layer is avoided.[6] Moreover, although challenging, *in situ* FTIR is possible when appropriate cell setups are used (Figure 6).[68,73–79]

It is worth mentioning that in order to increase the signal-to-noise ratio and to better visualise the changes in the peak intensity between subsequent spectra, the subtractive normalised interfacial FTIR technique (SNIFTIRS) can be successfully used.[6,74–75]

2.3.1. Limitations of FTIR

Considering that the interphases formed onto the electrode surfaces are thin layers, the vibration signals arising from its components may not be strong enough and therefore not very well resolvable. More importantly, the interpretation of the FTIR spectra is difficult considering that the components of the surface layers have often very similar functional groups. Therefore, interphase components with similar functionalities can cause overlapping vibrational signals within the spectrum, which become very challenging to deconvolute.[6] Even though *in situ* analysis is possible with an appropriate FTIR setup,[68,73–79] a major problem that the technique has to face in this configuration is the strong absorption of the electrolytes, which lowers the signal-to-noise ratio, and produces a CO_2 related peak within the spectrum as well. In this way, it becomes tricky to differentiate between the CO_2 signal related to the electro-

lyte and the one arising from carbonates-based species (e.g. Li_2CO_3) present in the interphase.[6,68,74,81] Moreover, it is difficult to perform a quantitative analysis based on the intensity of the peaks within the FTIR spectra, since the peak intensity is not only related to the amount of species present on the sample surface, but also to the nature of the chemical bond itself. In fact, more polar bonds give stronger signals than less polar ones.[6] Furthermore, some species among the principal components of interphase layers like LiF are infrared inactive.[6]

Concerning the substrates that can be analysed with FTIR it is worth mentioning that most of the electrodes of interest in lithium-ion batteries (which are based on particles of e.g. graphite, lithium metal oxides, olivines, etc.) do not reflect almost any IR light, and this results in a low signal-to-noise ratio. In order to overcome this limitation, the use of model systems like for example glassy carbon, metal oxides, single graphite particles, etc. with mirror-like polished surfaces is often invoked,[68,74–75,81] even though their behaviour may part from the one of the electrodes used in real-life Li-ion batteries.
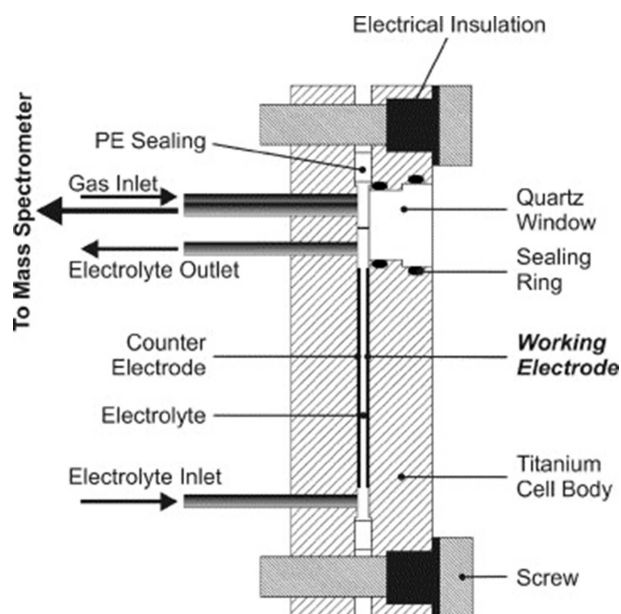
2.4. Differential Electrochemical Mass Spectrometry

Differential electrochemical mass spectrometry (DEMS) is a non-destructive tool used for the qualitative and quantitative analysis of the gaseous products generated during electrochemical reactions. In lithium-ion batteries, DEMS can be employed to study the gas evolution occurring upon the irreversible electrochemical decomposition of the electrolyte, thus investigating the reaction mechanisms of the SEI formation.[68,80,82] Its working principle is based on separating the ionised gaseous compounds according to their mass/charge ratio. In particular, gaseous ions are produced within an ion source, and successively separated into different mass-charge groups through the application of an electric or a magnetic field.[68]

One of the main advantages of such analysis is that it can be performed not only *in situ*, but also *operando*: the intensity change in the mass signals can be measured as a function of the time or the potential, thus allowing the correlation of the gas evolution to the peaks of a cyclic voltammetry or to the plateaus of a galvanostatic measurement. Moreover, with an opportune cell design, it is possible to analyse quantitatively the gas evolved, and to increase the detection limit to smaller amount of gas (Figure 7).[80,83–84] Another advantage of using this technique is related to its surface insensitivity, which allows the use of porous composite substrates, making DEMS analysis applicable to real-life battery electrodes. For this reason, DEMS experiments are helpful to elucidate the possible reaction mechanisms of the electrolyte decomposition leading to the formation of the SEI, and their potential dependence.[82,84]

2.4.1. Limitations of DEMS

Despite its many advantages, an accurate DEMS analysis strongly relies on the development of an appropriate cell, which is not trivial to be designed in such a way to ensure low

Batteries & Supercaps

Reviews
doi.org/10.1002/batt.201900177

Chemistry Europe
European Chemical
Societies Publishing

Figure 7. The electrochemical cell for in situ DEMS. Reprinted with permission from Ref. [80]. Copyright (2005) Elsevier.

noise and low gas detection limits. Moreover, DEMS analysis applied to the study of the SEI formation reactions has to be combined with other electrochemical and spectroscopic techniques, since the SEI formation does not always appear as a feature in the cyclic voltammetry (or in the galvanostatic curve) of the material. Furthermore, the decomposition of the electrolyte, to which gas evolution (e.g. CO_2, H_2, etc.[30,46,82–83]) is associated, does not necessarily ensure that a surface layer has been effectively formed onto the electrode's surface, and this is especially relevant for the study of the surface layer formed at the positive electrodes.

2.5. Electrochemical Impedance Spectroscopy

Electrochemical impedance spectroscopy (EIS) is an established, non-invasive electrochemical tool, which is routinely used to study, among other phenomena, the SEI formation and nature.[35,45,54] EIS is based on measuring the frequency response of an electrochemical system upon the application of a small potential difference over a wide range of frequencies. Taking into account its very non-destructive nature, EIS is a powerful *in situ* technique, which allows the observation of a large number of phenomena occurring in a broad range of time constants, and the interpretation of the current response of the system in terms of a physical model. Moreover, three-electrode measurements allow the investigation of single electrodes and of their degradation, also in terms of the SEI growth or of the mass loss.[85] Interestingly, it is also possible to measure impedance spectra *in-operando* through fast Fourier transform electrochemical impedance spectroscopy (FFT-EIS) or through dynamic multi-frequency analysis (DMFA),[86–88] thus looking at the phenomena *while* they are occurring.

2.5.1. Limitation of EIS

There are two main weak points that make EIS a difficult tool to handle: data acquisition and data interpretation.

Concerning the data acquisition, three electrode cells capable of acquiring impedance spectra at high frequency without distortions should be used, despite the fact that they are extremely difficult to build (Figure 8).[89–92] The geometrical position of the reference electrode with respect to the working electrode and the counter electrode is not a trivial aspect, and has a strong influence on the measured impedance spectra (Figure 9). Proper cells are very complex to build and unfortunately only rarely used. In addition, proper reference electrode's material has to be used.[93]

Two-electrode setups are certainly easier to handle and unfortunately widely used, but in this case, the response of both electrodes is summed up, and the contribution of the single electrodes on the recorded impedance is *nearly impossible* to separate. This makes the interpretation of the impedance spectra extremely complex, and leads to a misleading and often unrealistic interpretation of the phenomena occurring at the electrodes.

The interpretation of the impedance data is also not trivial. Impedance spectra are a way to measure the non-equilibrium behaviour of the electrochemical systems. A proper interpretation can be done only by fitting the results to a physical model. However, the often used equivalent circuits[35,45,54] lack of a proper correlation between the circuital elements and the physical meaning, thus becoming pure mathematical fitting parameters, without any physical correlation with the phenomena occurring in the system under analysis. Proper modelling of Li-ion batteries, which can be used for the interpretation of the impedance spectra, can be found in literature,[94–97] however they are only rarely used.
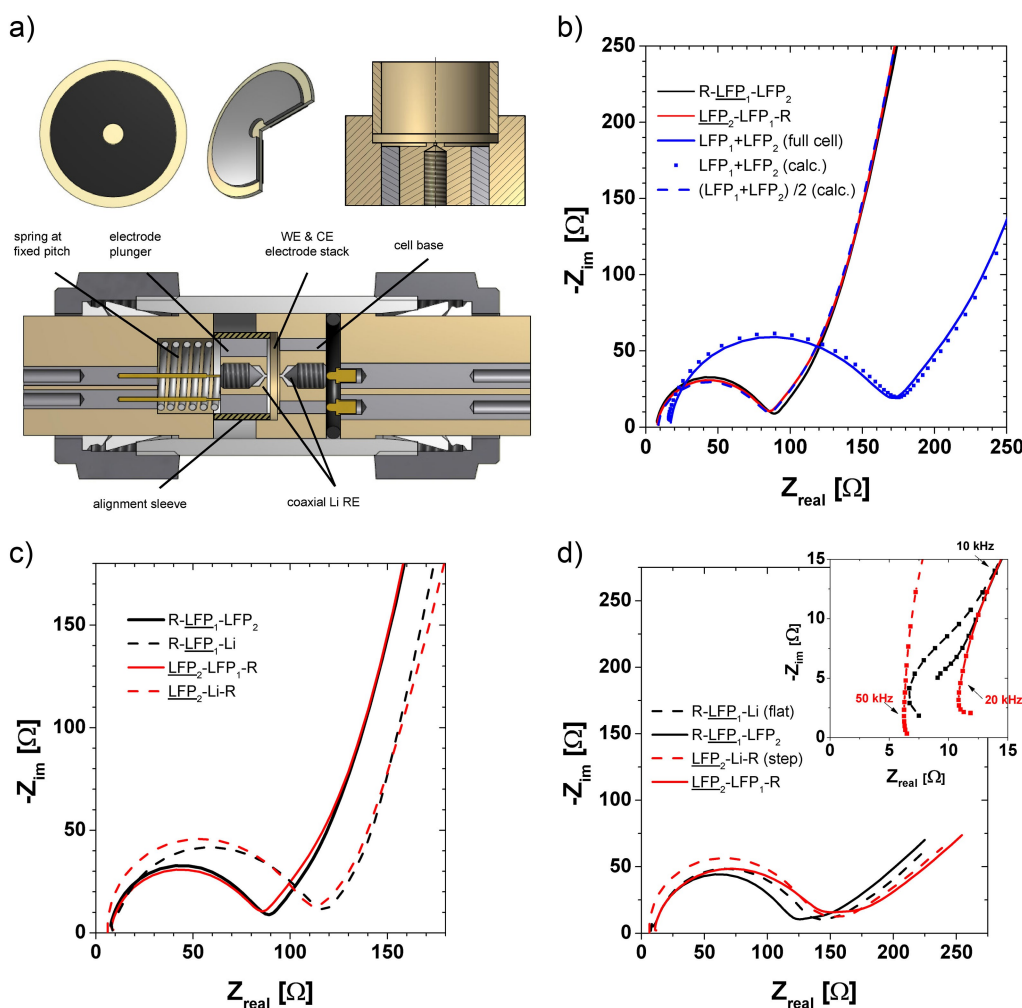
Last but not the least, the analysis of the statistical relevance of the parameters used for the fitting of the equivalent circuits, together with counter experiments at different conditions, is unfortunately rarely discussed at all.

All these points, which are *rarely taken into account* during EIS analysis of surface (and bulk) phenomena in Li-ion batteries, make the majority of the EIS measurements (and their interpretation) on the interphase available in the literature mostly untrustworthy.

2.6. Atomic Force Microscopy

Among the local probe techniques, atomic force microscopy (AFM) allows the acquisition of images of the surface under analysis with resolutions of a fraction of the nanometre. A sharp tip is positioned onto a thin cantilever, which is scanned along the surface under analysis. Deflections of the cantilever are related to the roughness of the surface, and allow the acquisition of 3D images of the surface topography.

Being the AFM a non-invasive, *in situ* tool, this technique has been used in lithium-ion batteries to monitor the morphology and growth of the interphase,[98] and to study its

Batteries & Supercaps

Reviews
doi.org/10.1002/batt.201900177

Chemistry
Europe
European Chemical
Societies Publishing

Figure 8. (Cell 3) a) improved coaxial cell with precise electrode alignment and defined spring pressure, suitable for thin separators like Celgard; fitted to $^3/_4$ in. Swagelok cells; 12 mm electrodes, i.d. 2 mm; 14 mm separator; cell is assembled from right to left; b) impedance spectra of two similar LFP electrodes (transferred from cell 2), 0% SOC; c) same electrodes, but separated and assembled with lithium CE, 0% SOC; d) same electrodes, at 50% SOC, with lithium CE and LFP CE. Reprinted with permission from Ref. [90]. Copyright (2012) Elsevier.
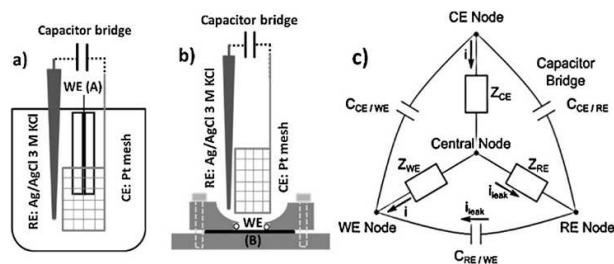
Figure 9. Sketches of the cell geometry: a) cell geometry A, b) cell geometry B. c) Schematic of the three electrode circuit with highlighted the capacitive coupling replaced by the capacitor bridge and the leakage current which produces the high frequency arc artefact in the EIS. Reprinted with permission from Ref. [92]. Copyright (2014) Elsevier.

structural stability at elevated temperatures.[99] Moreover, AFM can also be employed to estimate the surface layer thickness by scraping it off with the tip, and measuring the height difference between the scraped and the not-scraped areas of the electrodes.[98,100–101] Another way of employing AFM for the

interphase analysis in Li-ion batteries is through nanoindentation.[102–105] By pressing the AFM tip (of known mechanical properties) into the sample of unknown mechanical properties, it is possible to evaluate the Young modulus (i.e. elastic modulus), the hardness, and the strain-rate resistivity of the surface under analysis.

A further advantage of such analytical tool is that AFM measurements can be performed *in situ* and *operando*, thus providing information on the structure, thickness and mechanical properties of the interphases in their native environment.[101,103,105]

Through conductive AFM (c-AFM) it is possible to visualise the local electronic conductivity of the electrode, by employing an electronically conductive tip.[106] However, to our best knowledge there is no dedicated application to the visualisation of the SEI. In lithium-ion batteries, c-AFM has been used mainly to visualise local phase transformations occurring at the nanoscale,[106] Li$^+$ transport behaviours at grain borders and interiors,[107–108] and localised mechanical stress.[109]

2.6.1. Limitations of AFM

Despite its nanometre accuracy and the possibility of running the measurements *in situ* and *operando*, the reliability of AFM in terms of interphases thickness estimation has been recently challenged.[110–114] When estimating the SEI thickness with AFM, it has to be taken into account that part of the SEI might not be scratched away by the tip. As suggested from the compact stratified model,[12,15] the SEI could be constituted by an outer softer layer (i.e. the one closer to the electrolyte side) easier to be scraped off, and an inner harder layer (i.e. the one closer to the electrode side). This latter "underlayer" may actually remain on the electrode surface even after several scrapings[113] and, since it has been shown that its composition is different from the one of the pristine electrode,[115] it has been suggested that such underlayer may be the one responsible to a higher extent of the electronic insulating character of the SEI.[110–113] This latter hypothesis has been suggested also considering the sometimes-absent correlation between the electrochemical performance of the electrode, and the SEI thickness as measured by AFM.[110–113] This gives an idea of the complexity of the nature and the structure of such interphases, since the SEI quality is not necessarily correlated to its thickness.

When employed for the investigation of the interphase's mechanical properties, AFM suffers from the following limitations: (I) the Young's modulus can be generally estimated by assuming linear and isotropic materials,[105,116] which may not necessarily be the case for the interphases; (II) when soft materials are under analysis, like in the case of the interphase,[12] the experimental procedure suffers from intrinsic challenges related to the tip-surface adhesion and to the surface detection;[117] (III) the estimation of the mechanical properties of the substrate under analysis has been shown to be tip dependent.[105,116–117]

A further general disadvantage of employing AFM for the interphase analysis is related to the intrinsic local character of the experiment. Being the analysis restricted to grids of nanometric scale, it is difficult to use the collected local information to extrapolate the general behaviour of the electrode. In order to do so, the comparison of many measurements acquired in different areas of the electrode is generally advised, even though time consuming.

Last but not the least, AFM is generally applied to the study of flat electrodes or electrodes with a controlled roughness. For this reason, the application of AFM to the study of porous composite electrodes is not always straightforward, and this may result in errors in the data acquisition and interpretation.

## 3. Emerging Novel Analytical Techniques for the Interphase Investigation in Li–Ion Batteries

3.1. Scanning Electrochemical Microscopy

Another local probe technique is the scanning electrochemical microscopy (SECM), which measures the current of an electro-

chemical reaction occurring in correspondence of a microelectrode, often referred to as SECM tip (or SECM probe). The microelectrode is typically positioned close to the substrate surface under analysis. The perturbations of the electrochemical response of the SECM tip give information about the substrate nature and properties, and about the local reactions occurring in correspondence of the surface under analysis (Figure 10). Among the different SECM modes of operations,[118] SECM in the feedback mode can be employed to directly measure the electronic character of a surface, through the variation of the electron transfer kinetics of a free diffusive redox couple (the so-called redox mediator) present in solution in small amount. For this reason, feedback SECM has been for the first time employed[119] in lithium-ion batteries in order to visualise the SEI formation and insulating character.[119]

The unique feature of the feedback mode SECM of *directly* measuring the electronic insulating character of the SEI, is certainly one of the major advantages offered by such technique. Moreover, the interphase analysis can be performed *in situ* and *operando*, without altering the environment to which the battery electrode is exposed, thus avoiding any unwanted chemical change of the surface layer. By tuning the dimension of the microelectrode (i.e. SECM tip), information on both the local and the average behaviour of the electrode can be harvested.[119–121] Another advantage of such analysis lays in the fact that not only flat-finished surfaces but also porous composite electrodes can be used, thus allowing the *in situ* and *operando* study of the interphases formed onto real-life battery electrodes.

The SECM investigation of the interphases can be performed essentially in two different ways: (I) *operando*, by keeping the microelectrode at a fixed position, thus collecting time- and potential-resolved information about the interphase formation and changes during the polarisation of the Li-ion battery electrode;[119,121] (II) by moving the microelectrode over the substrate surface, thus obtaining *in situ* spatially resolved scans, in order to visualise the interphase formation and changes over time.[101,120,122]
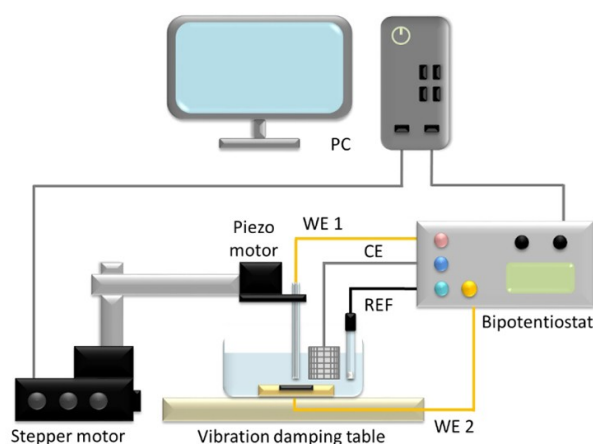
Figure 10. Schematic representation of the experimental apparatus of the scanning electrochemical microcopy.

Batteries & Supercaps

Reviews
doi.org/10.1002/batt.201900177

Chemistry Europe
European Chemical
Societies Publishing

In particular, the feedback mode SECM has been successfully employed to determine the SEI formation potential[101,119,121,123–124] and time stability,[120,122] the role of the Li^+ (and Na^+) cations in its insulating nature,[125] the SEI anodic stability[125] and the vinylene carbonate (VC) additive role on its formation potential and electronic nature.[126] Moreover, this technique has been very recently applied to *directly* visualise the electronic character of the interphases formed onto high potential positive electrodes.[65]

3.1.1. Limitations of SECM

Although the SECM can be operated within an Ar-filled glovebox for the *in situ* and *operando* analysis of the interphases, careful attention must be paid in the electrochemical cell design, which has to allow a homogeneous current lines distribution, in order to mimic the cycling conditions of the electrodes in conventional coin cells.[121] Moreover, the *operando* investigation of the interphases is usually limited during the first numbers of cycles of the Li-ion battery electrode (usually less than 10 cycles), in order to avoid a significant evaporation of the electrolytic solution. Even with a closed-cell design, the SECM electrochemical cell cannot be hermetically sealed,[119–121] and a small evaporation of the solvent occurs anyway over time. If too prolonged, the solvent evaporation can lead to changes in the concentration of the redox mediator present in solution, thus altering the electrochemical response collected by the SECM tip during the experiment.

In order to collect trustworthy data only related to the interphase, the permeability of the redox mediator employed for the feedback SECM analysis has to be evaluated. If permeable to the interphase, the electrochemical response collected at the SECM tip could reflect not only the surface layer, but also the bulk of the porous composite electrode and current collector. Moreover, it is worth pointing out that the redox mediator has to be chosen properly: it should be stable over the potential range applied during the polarisation of the Li-ion battery electrode, electrochemically reversible, chemically stable, and it should not influence the interphase formation and nature.

Finally, when the feedback SECM is employed to collect area scans of a portion of the surface, careful attention has to be paid when real porous composite electrodes are used. In this case, considering the high and irregular porosity and roughness of the porous electrode, the possibility of dragging the particles during the scan cannot be *a priori* ruled out. Last but not the least, from the area mappings collected through SECM it is not trivial to differentiate the contribution of the topography from the local reactivity of the sample.[118]

3.2. Neutron-Based Techniques

Neutron-based techniques such as neutron diffraction, scattering, and especially neutron reflectometry, have been recently applied to the *in situ* study of the interphases in lithium ion batteries in order to estimate their structure, thickness and composition.[127–130] The common denominator of the different neutron-based

techniques is the application of a thermal or cold beam of neutrons to the sample to be analysed.[131] The character of such analytical tool is purely non-destructive because of the low energy and neutral charge of the incident beam. The high resolution (especially for light atoms like Li), the non-destructive, highly penetrating nature of the neutron beam, and the possibility of performing measurements *operando*, allow a dynamic mapping of the SEI during the electrode charge/discharge, and provide information about its thickness.[129]

3.2.1. Limitations of neutron-based techniques

Being nuclear reactors the source of neutrons, the instrumental setup required to perform neutron-based analysis suffers from limited availability and high costs related to the experimental apparatus itself and its maintenance. This remains the major hindrance to the spread of neutron-based techniques. The development of a cell setup is extremely difficult, thus hindering the employment of the NMR-based analysis *operando*. Moreover, when performed *operando* a two-electrode cell setup is usually preferred (over a three-electrode one), even if information on the exact working electrode's potential is lost. In addition, despite the big potential that this analytical tool offers, in terms of the variety of information that can be collected in a non-destructive way about the surface layer, the massively stringent restrictions on the roughness of the surface under analysis[129] severely limit the applicability of the neutron-based techniques to real-life battery electrodes.

3.3. Ellipsometry

Ellipsometry is a surface sensitive optical technique, which measures the change of polarisation of a smooth surface upon the reflection or the transmission of a linearly polarised light beam. Information regarding the surface roughness, density, and dielectric properties of the sample's surface can be derived through the development of appropriate models.[132–134] In lithium-ion batteries, ellipsometry has been applied to the study of the SEI thickness[134] and density,[135] and to study the decomposition mechanism of organic electrolytes.[132–133] Non-destructive character of the incident beam, high accuracy and possibility of performing experiments *in situ* make this analytical tool very attractive for the study of Li-ion battery interphase layers in their native environment.

3.3.1. Limitations of ellipsometry

Even if this technique would be ideal to estimate the interphase thickness with a high accuracy, and to monitor its growth thanks to the non-interfering nature of the light beam, the instrumental setup is generally applied *ex situ*, since the development of an *in situ* electrochemical cell is not trivial. Moreover, such methodology requires the development of reliable models for the data interpretation, and the use of

Batteries & Supercaps

Reviews
doi.org/10.1002/batt.201900177

Chemistry
Europe
European Chemical
Societies Publishing

samples with a very smooth surface, which are far from the real (highly porous) battery electrodes.

3.4. Fluorescence Microscopy

A particular kind of optical microscope is the fluorescence microscope, which employs fluorescence and phosphorescence instead of (or in addition to) scattering, reflection, etc., to study inorganic and organic compounds. The substrate under analysis is illuminated with light of a specific wavelength, which is absorbed by the fluorophores and re-emitted with a longer wavelength.

In Li-ion batteries, fluorescence microscopy can be used to track lithium ions inside the battery system (Figure 11a).[136–137] Moreover, some recent efforts have been directed to the application of fluorescent microscopy to the study of the fluorescent species produced at the positive electrode/electrolyte interface when high anodic potentials are reached (Figure 11b).[138–140]
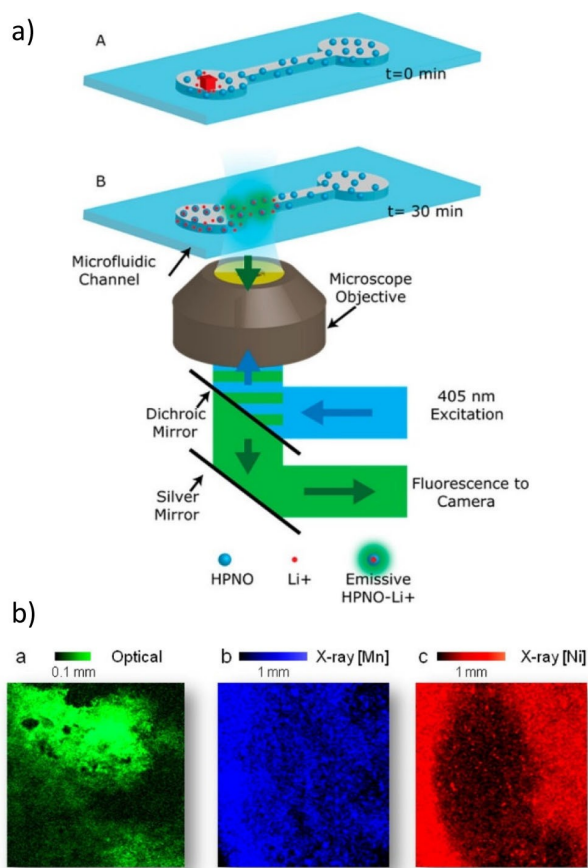
Figure 11. a) (*A*)Schematic of a PDMS microfluidic channel immediately after a LiCl crystal (red cube) is placed at one end. (*B*) Using widefield fluorescence microscopy, the flow of lithium ions can be tracked as lithium ions bind to 1, making it fluorescent under excitation. Reprinted with permission from Ref. [136]. Copyright (2017) American Chemical Society. b) Optical and X-ray fluorescence images of the graphite negative electrode from a tested Li-ion cell. (*a*) Optical fluorescence image (488 nm excitation). (b, c) XRF maps of the (*b*) Mn and (*c*) Ni elemental distributions ($\lambda_{ex} = 8500$ eV). Reprinted with permission from Ref. [139]. Copyright (2015) American Chemical Society.

This technique can be employed *in situ* to identify the preferential sites of the electrode surface at which the oxidation reaction occurs,[141] together with the fluorescent species produced from the dissolution of the metallic constituents of the positive electrodes. These species can travel through the battery during several charge/discharge cycles and, reaching the negative electrode side, can be included in the SEI on the negative electrode, influencing its chemical nature and properties.

3.4.1. Limitations of fluorescence microscopy

This analytical technique, despite its high resolution, provides no information on the structure and/or on the physicochemical nature of the interphases. Moreover, it is generally employed *ex situ* and only fluorescent/phosphorescent species can be visualised. Even though fluorescence indicators can be synthesised and used to tag the non-fluorescent species of interest,[136] the introduction of such indicators can affect the already complex formation mechanism of the interphases, thus changing its composition or physicochemical nature. Finally, most of the fluorescent species that can be visualised remain of unknown composition.[140]

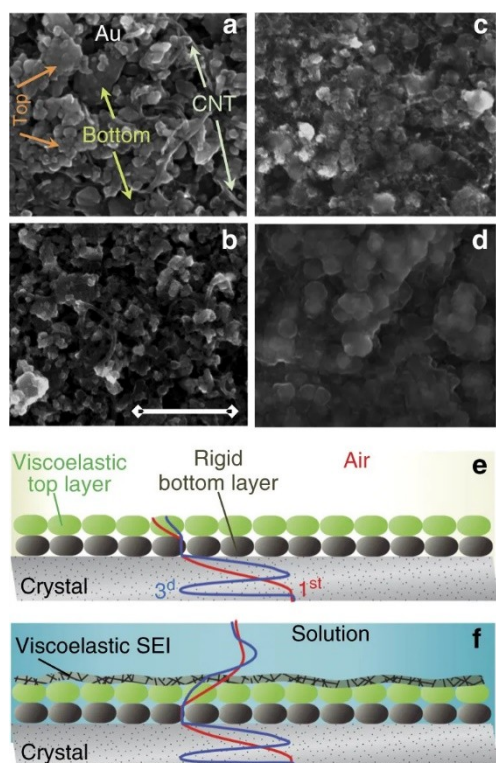## 3.5. Electrochemical Quartz Crystal Microbalance

The electrochemical quartz crystal microbalance (EQCM) is an *in situ* gravimetric analytical tool that allows the determination of the mass changes (accumulation or decrease) during the electrochemical reactions taking place at an electrode. The sample under analysis is mounted onto a piezo quartz crystal, and through the monitoring of the crystal vibrations, it is possible to correlate the mass changes to the electric charge flow.[142] Depending on the setup employed this technique can be employed *operando*, it has a non-destructive nature, and it can be applied to the study of porous, real-life battery electrodes.

In lithium-ion batteries, EQCM has been used to quantitatively study ion adsorption,[143] material deformations caused by the Li$^+$ intercalation in porous electrodes,[144] and to study the interphase formation,[145] viscoelastic properties,[146] and the role of the additives to its composition and thickness[147] (Figure 12). EQCM analysis of the interphases give quantitative information regarding (I) the viscosity and the ion conductivity changes near the electrode during its cycles,[148] (II) the potential range of the main mass accumulation (related to the interphase formation),[145] and (III) the influence of the electrolyte components (in terms of solvents, salts and additives) on the possible interphase thickness.[147]
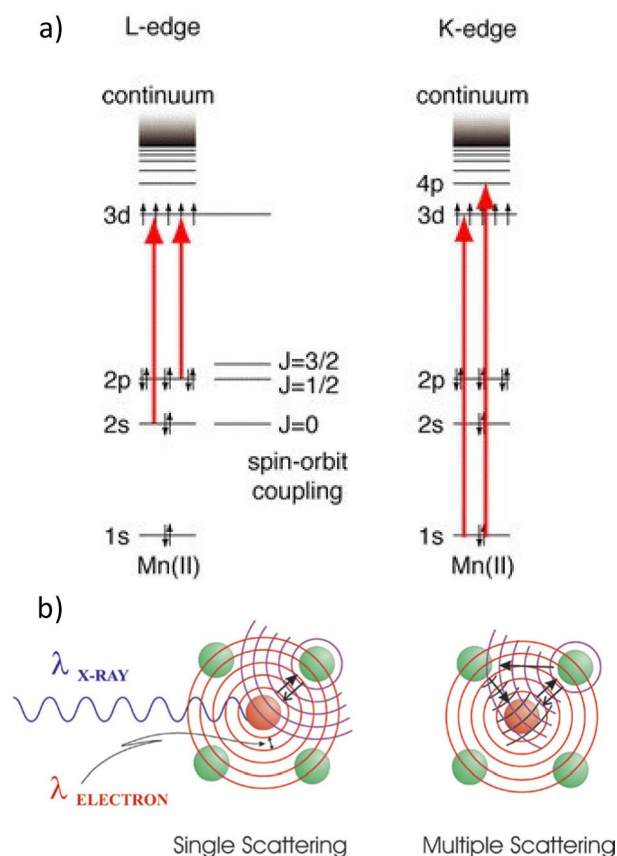
3.5.1. Limitations of EQCM

During EQCM measurements, the mass per charge ratio should ideally reflect the stoichiometry of the electrochemical processes taking place at the electrode, however this is not always the case when EQCM is applied to the study of the Li-ion

Batteries & Supercaps

Reviews
doi.org/10.1002/batt.201900177

Chemistry Europe
European Chemical
Societies Publishing

Figure 12. SEM images of LTO electrodes on quartz-crystal surface and their model presentation. a) pristine electrode, b) cycled in EC-DMC 1 M LiTFSI, c) 1 M $LiPF_6$, and d) 1 M $LiPF_6$ + 2% VC solutions (scale bar = 500 nm). e) Sketch of velocity profiles for rigid and viscoelastic layers of LTO electrodes in air and f) in electrolyte solution. Velocity profile of shear wave crossing the multilayer assembly is exemplified for fundamental frequency and third overtone order. Reprinted from Ref. [146]. Copyright (2017) The Authors.

Figure 13. a) The energy level diagram for L-edge (L_I, L_{II}, and L_{III}) transitions (2s and 2p to 3d) and K-edge transitions (1s to 3d and 4p) for Mn(II). The energy levels are not drawn to scale. For example, the K-edge is at 6,539 eV and the L edges are at 769, 650, and 639 eV, respectively. Reprinted with permission from Ref. [154]. b) pattern of an outgoing and backscattered photoelectron wave in the case of EXAFS (single scattering events) and XANES (multiple scattering events). Reprinted with permission from Ref. [155]. Copyright (2004) American Chemical Society.

batteries interphases. As a matter of fact, most of the times the mass per charge does not correspond to any species that should be present within the interphase,[147] or it is actually smaller than the one that the components detected within the interphase through other *in situ* techniques should have.[149]
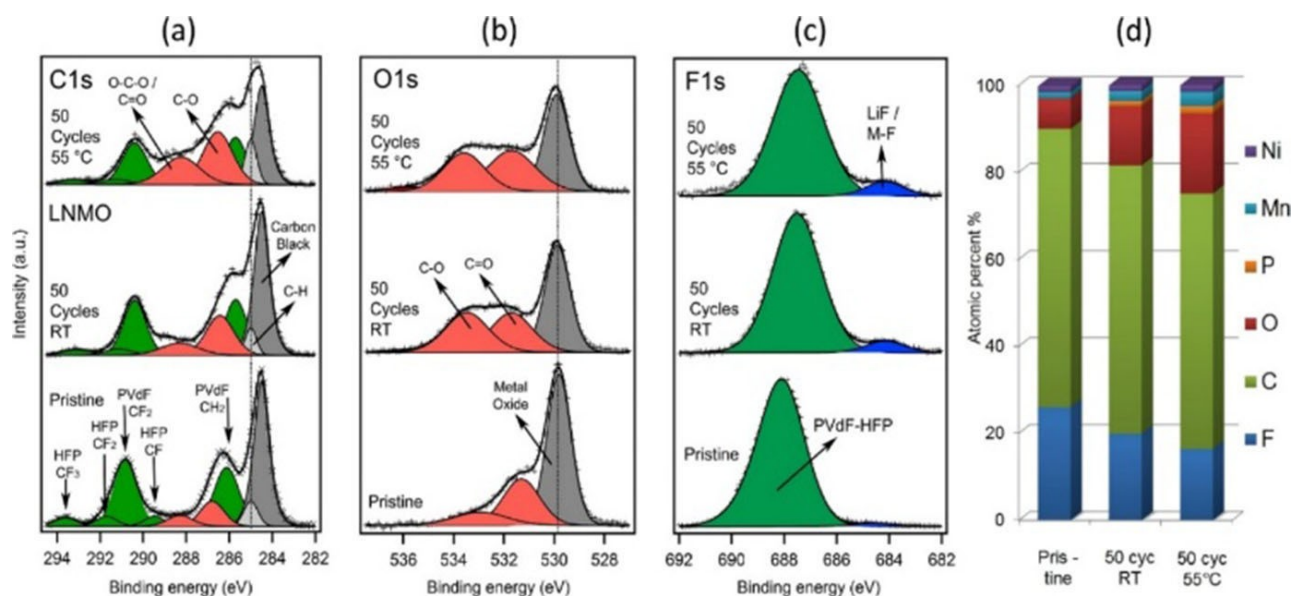
In order to be conclusive, any unwanted changes in the dissipation factor should be carefully avoided, and the electrode under analysis should always be rigidly fixed onto the crystal, both at open circuit and during the application of a potential.[142] Moreover, particular attention should be paid to the crystal oscillation frequency changes given by multiple parasitic processes, such as asymmetrical mechanical stress,[135] viscosity changes in the solution near the surface of the electrode,[150] temperature variations,[151] and unwanted chemical reactions.[151] Such parasitic processes may introduce severe errors in the analysis, thus hindering the extraction of reliable quantitative data. Moreover, in order to achieve a correct interpretation of the acquired data, the roughness and porous structure of the electrode surface has to be taken into account through the development of adequate models.[151–153] This last aspect is highly important in order to investigate the behaviour of electrodes that approach the porous composite ones employed in real-life Li-ion batteries.

3.6. X-ray Absorption Spectroscopy

Another technique that has recently found its application in the frame of the interphase analysis in Li-ion batteries is the X-ray adsorption spectrometry (XAS). XAS employs X-rays in order to gather information on the local structure of the material under analysis, being it a molecule or an atom. This technique allows measuring the X-rays absorption as a function of the energy of the incident X-ray beam.[154–155] In this way, the variations of the absorption coefficient are detected, which are characteristic of a specific absorbing element, and are related with the energies required for the transition of an electron from the core atom to an unoccupied level (LUMO) or to the continuum (ionisation) (Figure 13a). Depending on the type of the electronic transition recorded, one can refer to X-ray absorption near-edge spectroscopy (XANES), and to extended X-ray absorption fine structure (EXAFS). In particular, XANES spectra are useful to gather detailed qualitative and quantitative information on the oxidation state, site symmetries, and covalent bond strength of the probed species,[154–155] whilst EXAFS spectra provide information on the local environment of

Batteries & Supercaps

Reviews
doi.org/10.1002/batt.201900177

Chemistry
Europe
European Chemical
Societies Publishing

Figure 14. a) C 1s, O 1s, and F 1s XPS spectra of pristine and cycled LNMO electrodes. Reprinted with permission from Ref. [166]. Copyright (2018) American Chemical Society.

the probed species, in terms of coordination numbers, bond length, and chemical nature of the neighbouring atoms[154–155] (Figure 13b).

In the frame of lithium-ion batteries, XAS has been used for investigating: (I) the reaction mechanisms, phase changes, and degradation processes occurring at the electrodes' surface (up to a depth of c.a. 3 nm) and bulk (up to a depth of c.a. 100 nm) of the active material;[156–159] (II) the change in the oxidation state of the metallic ions constituting the active material;[157,160] (III) the formation mechanism(s) and the chemical nature of the components of the surface layers.[158–159,161–162] Beside XANES and EXAFS, also soft XAS and total-reflection fluorescence TRF-XAS (both synchrotron-based) have been employed for the interphase analysis.[158–159,161–162]

The main advantages of XAS are related to: (I) the possibility to perform measurements *in situ*, and to deliver both electronic and structural information; (II) its high selectivity, allowing to measure very diluted samples; (III) its very high precision, which is in the order of $10^{-2} \sim 10^{-3}$ Å for the structural determination, allowing the observation of transient structures of reaction intermediates.[154–155,157]

3.6.1. Limitations of XAS

General XAS limitations are related to: (I) the fact that the technique works best with ordered and/or highly concentrated samples; (II) the sample can undergo photochemical and/or laser induced damage; (III) in order to obtain full structural information a great number of Bragg reflections needs to be monitored, making the data interpretation not trivial.[154–155]

In addition to the aforementioned limitations, other aspects need to be considered when XAS is applied to the interphase analysis. The cell for the *in situ* analysis is not straightforward to
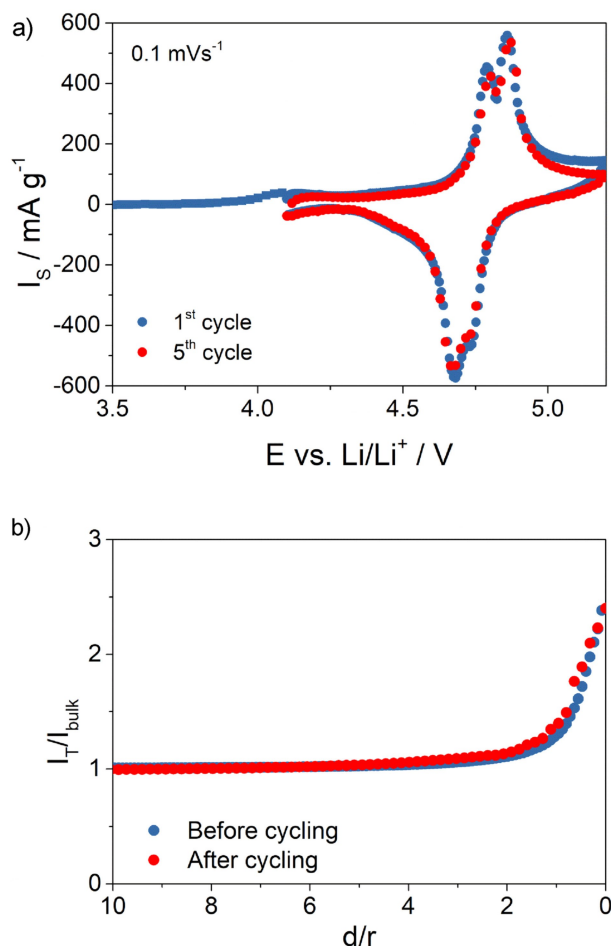
design, and its employment requires careful attention in the calibration of the penetration depths of the incident beam. Moreover, in order to achieve the high sensitivity and precision needed for the surface layer's analysis, synchrotron has to be used as beam source. As a consequence, the use of high energy photons and ultrahigh vacuum conditions may alter the composition and/or partially decompose the surface layer under investigation. Last but not the least, even considering that the technique has been also applied to the study of porous battery electrodes, flat-finished polycrystalline thin film electrodes are preferred for this kind of analysis in order to achieve high resolution,[156,159] thus limiting the application of the technique to real-life Li-ion battery electrodes.

4. Surface Layers on High-Voltage Positive Electrodes

As briefly stated within the scope of the review (Section 1.3) we will give an overview of what has been reported so far regarding the surface layers formed onto high operating voltage positive electrodes for high energy Li-ion batteries. In particular, we will focus on lithium nickel manganese oxide, lithium nickel manganese cobalt oxide, lithium nickel cobalt aluminium oxide, and on the inactive electrode components (i.e. conductive carbon, binder and aluminium current collector).

Despite polyanionic compounds (such as $LiNiPO_4$, $LiCoPO_4$, $Li_3V_2(PO_4)_3$, etc.) can be cycled up to potentials reaching $4.8 \sim 5$ V vs. Li/Li$^+$,[163–165] to the best of our knowledge there are no studies dedicated to the interphase analysis that may be forming on these materials. The reason for this could be related to the fact that this class of materials, although very promising
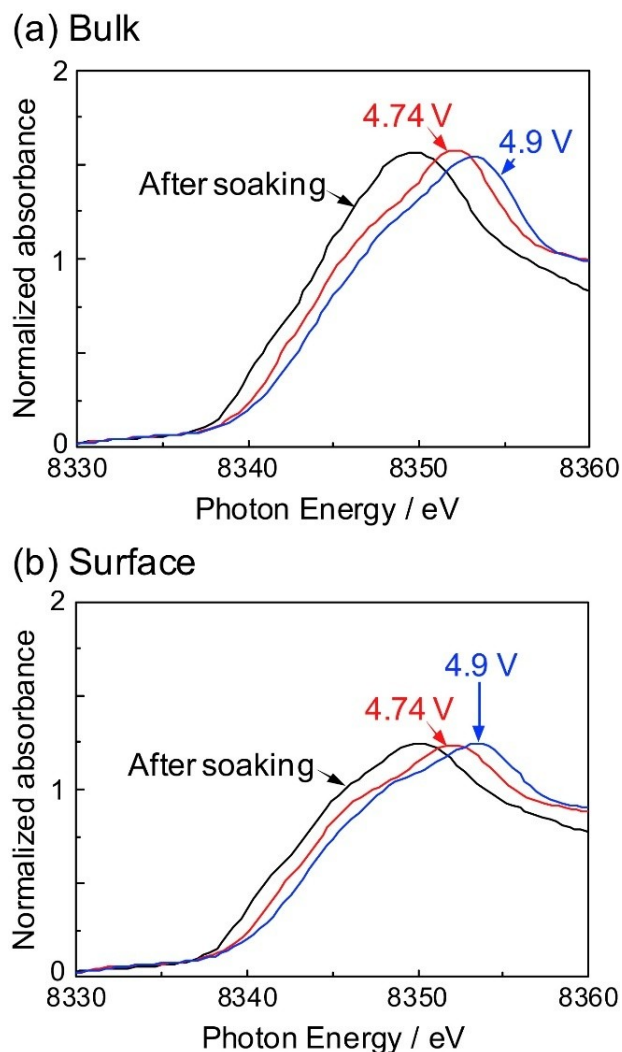
Batteries & Supercaps

Reviews
doi.org/10.1002/batt.201900177

Chemistry Europe
European Chemical
Societies Publishing

Figure 15. a) Cyclic voltammogram of a $LiNi_{0.5}Mn_{1.5}O_4$-based paste electrode in 1 M $LiPF_6$ EC:DEC (1:1 wt%). b) z-Approach curves (r: radius of the tip: 12.5 mm; d: tip-to-sample distance) to the $LiNi_{0.5}Mn_{1.5}O_4$ surface before and after the cyclic voltammogram in 15mMFcPF61M $LiPF_6$ EC:DEC (1:1 wt%). Paste electrode held at OCP (4.1 V); applied tip potential: 3.0 V. Reprinted with permission from Ref. [65]. Copyright (2017) PCCP Owner Societies.

Figure 16. Ni K-edge TRF-XAS spectra of the LiNi0.5Mn1.5O4 thin-film electrodes after the electrolyte soaking, at 4.74 V and at 5.0 V from a) the bulk and b) the surface, respectively. Reprinted with permission from Ref. [159]. Copyright (2013) Elsevier.

for electromobility applications, is still an early stage of development.

Since the surface layer formed upon the irreversible electrolyte oxidation is foreseen to play a key role in enabling the use of the next generation of high energy Li-ion batteries, we will not focus on the materials operating at potentials lower than 3.5 V ~ 3.7 V vs. Li/Li^+ (such as for example $LiCoO_2$ and $LiFePO_4$). In order to collect more information on the surface layers formed (if any) onto the electrode materials used in Li-ion batteries for portable electronic applications, we suggest the readers to refer to the following reviews and reports.[17,32]

4.1. Lithium-Nickel-Manganese Oxide (LNM)

$LiNi_{0.5}Mn_{1.5}O_4$ is a promising spinel for high energy density Li-ion batteries, considering its charge capacity of 148 mAhg^{-1} and its operating potential of c.a. 4.7 V vs. Li/Li^+.[10] Several studies based on XPS, FTIR, TEM, EIS, have reporte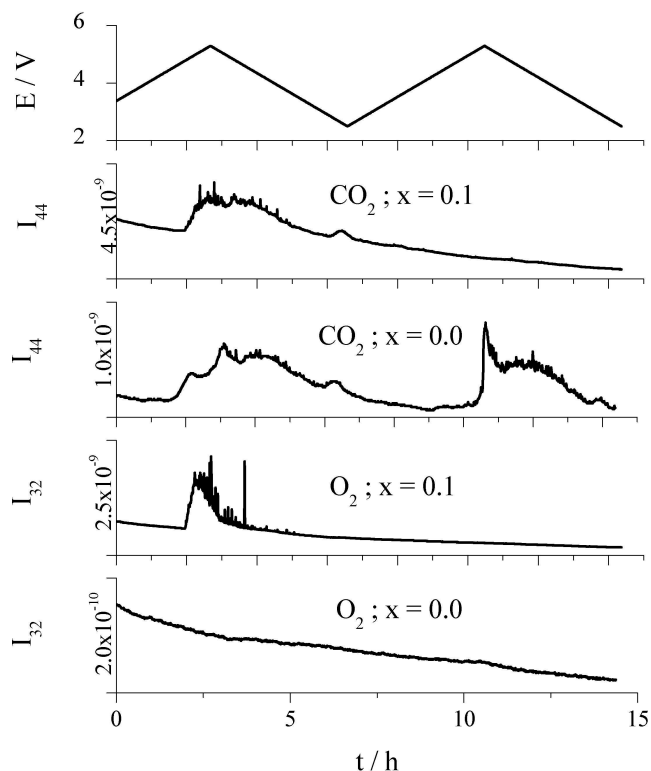d a surface layer formation during the initial cycles of the electrode,[32,34–35,166] with thickness increasing upon increasing the number of cycles.[42,167] Such surface layer appears mainly constituted of inorganic salts (among which LiF), polycarbonates and polyethers[63,166–168] (Figure 14).

However, the mechanism of its formation remains unclear. As an example, XPS studies of LNM thin film cycled in a solution containing 1 M $LiPF_6$ EC:DMC (1:1) found no product of the electrolyte decomposition, suggesting that the surface layer could be formed preferentially onto the inactive components of the paste composite electrode.[169] In contrast, FTIR studies of LNM thin film electrodes, cycled in the same solution as in Ref. [169], detected electrolyte decomposition products even at low electrode polarisations, suggesting that, at least in part, the surface layer could be formed chemically upon direct contact with the electrolyte.[170]

Also concerning the physicochemical characteristics of the surface layer formed on LMN electrodes no definite agreement has been reached: in EC:DMC-based solutions XPS, FTIR and EIS

Batteries & Supercaps

Reviews
doi.org/10.1002/batt.201900177

Chemistry
Europe
European Chemical
Societies Publishing

Figure 17. Plot of mass signal intensities Im/z [A g^{-1}] for $Li_{1+x}(Ni_{1/3}Mn_{1/3}Co_{1/3})_{1-x}O_2$ ($x=0$ and $x=0.1$, respectively) normalized in respect to the oxide mass; E is the potential vs. Li/Li$^+$ [V]. Reprinted with permission from Ref. [30]. Copyright (2008) Springer Nature.

Figure 18. Evolution of the cell parameters of $Li[Li_{0.2}Mn_{0.61}Ni_{0.18}Mg_{0.01}]O_2$ during cycling (first three sweeps). Reprinted with permission from Ref. [182]. Copyright (2012) Royal Society of Chemistry.

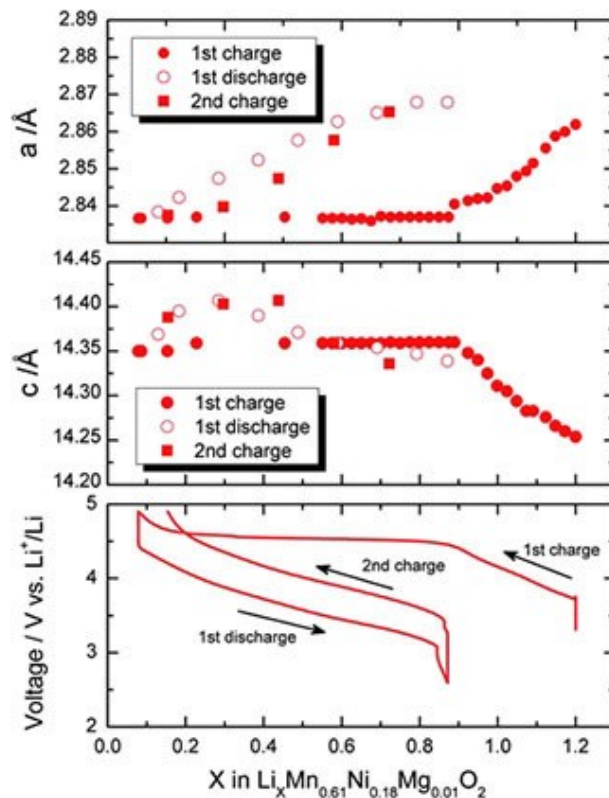studies suggested the formation of a protective surface layer[63] also at elevated temperatures (70 °C).[171]

In EC:DEC based solutions SECM studies directly probed the formation of an electronically conductive layer[65] (Figure 15), and later XPS studies proposed the formation, in the same solution, of a layer permeable to the solvent molecules, thus not preventing the electrolyte irreversible oxidation.[172]

As for the thin films of LNM when cycled up to 4.9 V vs. Li/Li$^+$ in 1 M LiClO$_4$ EC:DEC (1:1), *ex situ* XPS studies revealed the presence of a surface layer constituted of carbonyl and/or carbonate species (likely lithium alkyl carbonates).[159] However, *in situ* TRF-XAS measurements showed on the same electrodes that the chemical state and the local environment of the LNM surface was the same as the one in the bulk of the polycrystalline thin film (Figure 16). Therefore, in this case it has been suggested that the surface layer formed upon the irreversible electrolyte oxidation does not influence the surface composition of the LNM.[159]

A further, more systematic investigation is required in order to gain a clearer and less contradictory understanding of the surface layer formed onto LNM.

4.2. Lithium-Nickel-Manganese-Cobalt Oxide (NMC)

$Li_{1+x}(Ni_{1/3}Mn_{1/3}Co_{1/3})_{1-x}O_2$ (NMC)-based positive electrodes are employed in commercial Li-ion batteries, usually in combina-

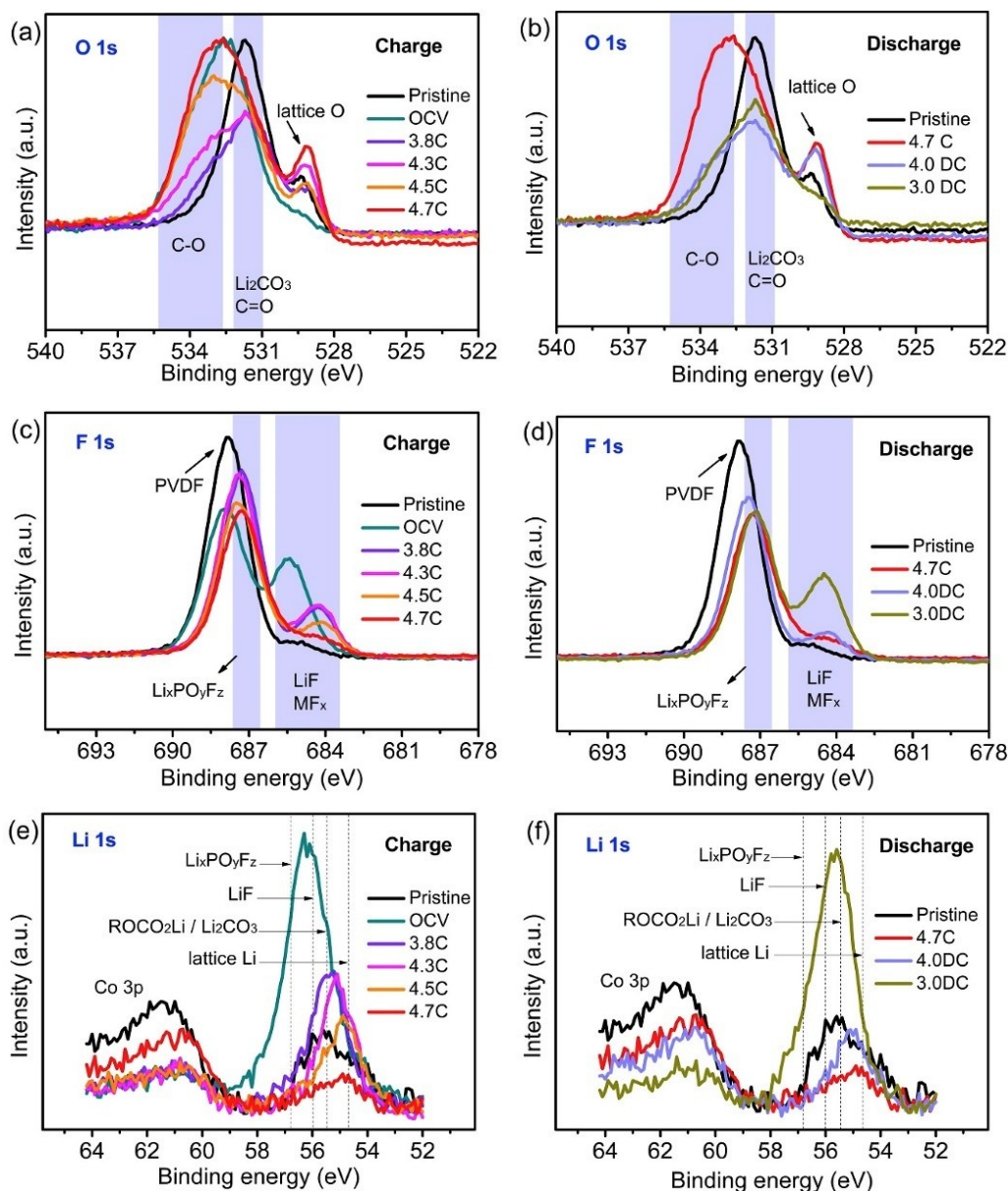tion with graphite-based negative electrodes. Such materials are promising candidates for high energy density Li-ion batteries for electromobility applications, thanks to their highly anodic operating potential (3.7–4.5 V vs. Li/Li$^+$)[30,173–174] and charge capacity (around 200 mAh/g).[173]

Several investigations, based mainly on XPS and DEMS,[30,173–180] have suggested the formation of a surface layer on NMC electrodes cycled at various potentials in contact with different solvents.[30,65,173–180] Such surface layer is supposed to be composed of organic carbonates and inorganic salts such as LiF, Li_2CO_3, together with phosphorous containing species.[176–177,179–180] However, there is still a lack of agreement concerning the formation mechanism of such surface layer. In solutions containing 1 M LiPF$_6$ EC:DEC (1:1) it was suggested that the surface layer may be built up appreciably only by repeated cycling,[176] whilst in 1 M LiPF$_6$ EC:DMC (1:1) a surface layer was detected on NMC during its initial cycling, suggesting that the active material may react itself as a reagent for the electrolyte decomposition, when oxygen is released from its lattice.[180]

Regarding the physicochemical nature of this surface layer, DEMS studies suggested that the layer formed onto stoichiometric NMC (i.e. $Li_{1+x}(Ni_{1/3}Mn_{1/3}Co_{1/3})_{1-x}O_2$ where $x=0$) based electrodes is expected to be electronically conductive. Such hypothesis was based on the continuous detection of CO_2, evolving from the anodic decomposition of the EC:DEC (1:1) based electrolyte during the first several cycles (Figure 17).[30] The electronic conductive character of the surface layer formed

Batteries & Supercaps

Reviews
doi.org/10.1002/batt.201900177

Chemistry
Europe
European Chemical
Societies Publishing

Figure 19. XPS spectra of NMC at different voltages in the first cycle (a–b) O 1s, (c–d) F 1s, and (e–f) Li 1s. Reprinted with permission from Ref. [158]. Copyright (2019) Elsevier.

on stoichiometric NMC operated in the same EC:DEC based solution was confirmed by later SECM studies.[65]

For over-lithiated NMC (i.e. $Li_{1+x}(Ni_{1/3}Mn_{1/3}Co_{1/3})_{1-x}O_2$ where $x=0.1$), DEMS studies performed in EC:DEC based solutions suggested the formation of an electronically insulating surface layer. Such conclusion was based on the observation of the CO_2 evolution, which comes from the decomposition of the electrolyte, occurred only during the first cycle,[30,174] together with O_2 evolution[30,174] (Figure 17). Oxygen radicals are in fact released from the over-lithiated NMC lattice, because of its structural changes occurring during the first Li^+ deinsertion[174,181–182] (Figure 18). The CO_2 evolution suppression was thus ascribed to the insulating character of the surface layer, preventing any further electron transfer from the electrode to the

electrolyte.[30,174] Such insulating surface layer was suggested to be the result of both the high anodic polarisation of the NMC electrode (up to 5.25 V vs. Li/Li$^+$), and the reaction of the oxygen radicals with the electrolyte.[30,174] However, direct SECM experiments resulted in the observation of an electronically conductive surface layer, also for the over-lithiated NMC, cycled in the same potential range and electrolyte.[65] The hindrance of CO_2 evolution was thus suggested to occur because of the catalytic effect of the NMC surface, when undergoing structural changes during the release of oxygen radicals.[65]

Recent XPS studies performed *ex situ* during the initial cycling of $LiNi_{0.6}Co_{0.2}Mn_{0.2}O_2$ in 1 M $LiPF_6$ EC:DEC (1:1) report a dynamic nature of the surface layer formed when the material was cycled up to 4.6 V vs. Li/Li$^+$ (Figure 19). In particular, the
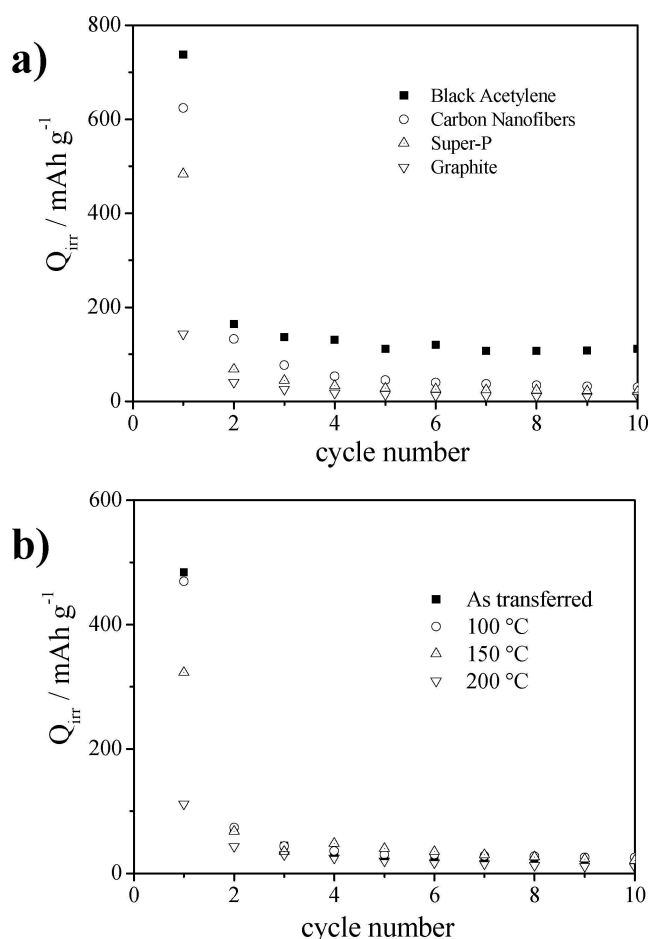
Figure 20. Irreversible-specific charge versus cycle number. a) Carbon additives, cell assembled immediately after the transfer in the glow box. b) Super-P after different thermal treatments for 3 h in glove box. Reprinted with permission from Ref. [185]. Copyright (2012) Springer Nature.
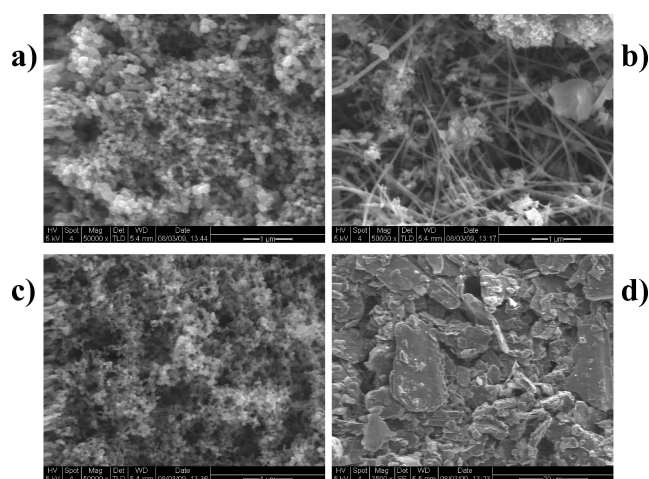
Figure 21. SEM pictures of the carbon powders. (a) acetylene black; (b) carbon nanofibers; (c) Super-P; (d) graphite. Reprinted with permission from Ref. [185]. Copyright (2012) Springer Nature.

accumulation of species such as lithium fluoride and lithium carbonates was observed to form upon direct contact of the

NMC-based electrode with the electrolyte.[158] Moreover, such initial surface layer was reported to be continuously formed and dissolved upon the charge and the discharge of the electrode. *Ex situ* XAS analysis on the same NMC electrodes demonstrated the formation of inactive species on the electrode's surface, which are supposed to further hinder the Li⁺ transport and to reduce the concentration of the active sites available for the Li⁺ (de-)insertion.[158]

A clearer understanding of the formation and nature of the surface layers formed on NMC-based electrodes would enable their use to higher anodic potentials, thus allowing an increase of the energy density of the Li-ion cell.

4.3. Lithium-Nickel-Cobalt-Aluminum Oxide (NCA)

$LiNi_{0.8}Co_{0.15}Al_{0.05}O_2$ (NCA), with an operational range up to 4.2 V vs. Li/Li⁺ and an average charge capacity of c.a. 200 mAhg⁻¹, is another promising active material for high energy Li-ion batteries.[183] Unfortunately, NCA suffers from degradation upon cycling up to 4.5 and even up to 4.2 V vs. Li/Li⁺, involving an irreversible damage of its structure and chemical composition.[183–184] Despites such material is generally used for the Li-ion battery of commercial portable electronic devices,[183] and the fact that NCA-based electrodes are potential candidates for high energy LIB applications, there are only few studies related to the surface layer that may be forming during its cycle life.

An *ex situ* study through scanning transmission electron microscopy (STEM) and electron energy loss spectroscopy (EELS) was performed onto a commercial NCA-based Li-ion battery with $LiPF_6$ as electrolyte cycled for 150 cycles up to 4.2 V vs. Li/Li⁺.[183] The STEM and EEL analysis demonstrated the formation of a thick layer of c.a. 10 nm of "degraded surface layer". Such degraded surface layer was constituted of Ni_yO_x (resulting from phase and structural transformations of the NCA). In addition to this, *ex situ* XPS analysis demonstrated the presence of Li_2CO_3 within such surface layer,[183] which might result from the electrolyte oxidation. However, having been the XPS analysis carried out *ex situ*, the possibility of the Li_2CO_3 coming from a contamination of the samples with a small amount of air during the transport step from the glovebox to the XPS vacuum chamber[70–71] cannot be completely excluded. Another study based on *ex situ* SEM showed that onto the surface NCA cycled 1 M $LiPF_6$ EC:DEC (1:1) up to 4.5 V vs. Li/Li⁺ a thick surface layer was present after 200 cycles. Even though no composition analysis was performed on the samples, *ex situ* SEM showed that the presence of an additive (a trimethylsilyl based malonate ester) prevented the deposition of such surface layer onto the NCA electrode's surface.[184]

As too few studies have been performed so far onto NCA electrodes cycled up to potentials high enough to promote a considerable irreversible oxidation of the electrolyte, there is a great lack of information regarding the physicochemical nature of the surface layer and its role on the cycle life of NCA-based Li-ion batteries.
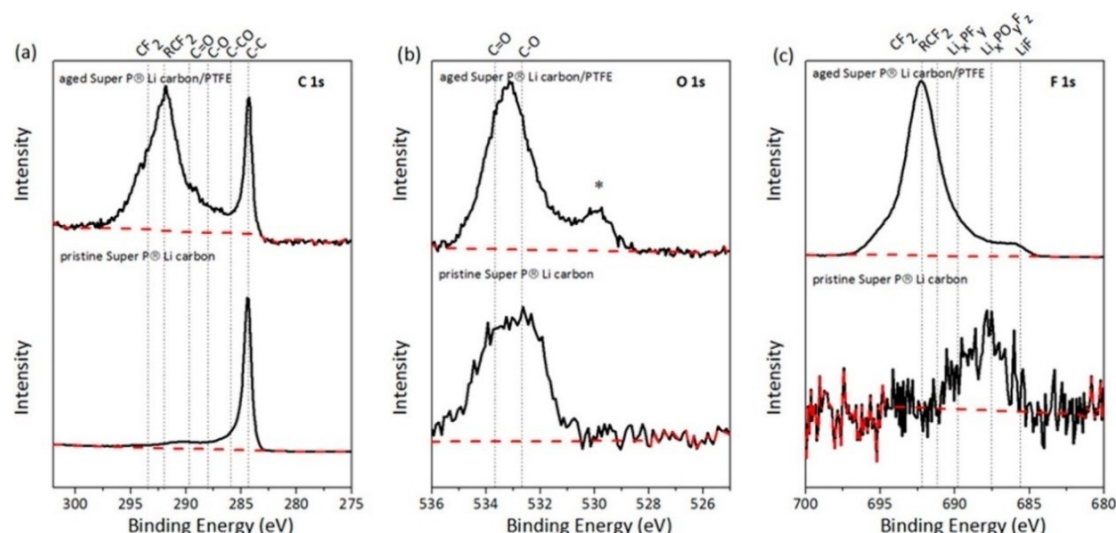
Figure 22. a) C 1s, b) O 1s, and c) F 1s spectra of pristine Super P Li carbon compared to Super P Li carbon/PTFE after being aged in 1 M LiPF$_6$ in a 1:1 EC/DEC electrolyte for 60 days showing the spontaneous formation of the SEI. Unknown species denoted with asterisk. Reprinted with permission from Ref. [33]. Copyright (2015) American Chemical Society.

4.4. Inactive Electrode Components

Considering the fact that the irreversible oxidation of the electrolyte is influenced by the material constituting the electrode under analysis, it is of importance to understand whether these irreversible processes occur preferably (or even selectively) onto the inactive electrodes components, namely: the carbon additive particles, the polymeric binder and/or the aluminium current collector, as suggested in Refs. [169, 179].

4.4.1. Conductive carbon additive and polymeric binder

It has been shown that the nature of the carbon additive influences the irreversible oxidative reactions of the electrolyte[33,179,185] (Figure 20). In particular, it has been suggested that the extent of the irreversible charge (Table 2) observed during the cycling of the electrode is not correlated to geometrical effects, considering the similar morphology of different conductive carbon additives (Figure 21), but rather to the nature of the conductive carbon additives themselves, in terms of surface groups.[185] It is worth mentioning that the nature of the surface groups present on the conductive carbon additives is strongly related to their synthesis conditions.[185]

Table 2. Characteristics and irreversible charge for the different carbon additives investigated. Q_{irr} and q_{irr} are the specific irreversible charge and the density of irreversible charge with respect to the BET area, respectively. Adapted with permission from Ref. [185]. Copyright (2012) Springer Nature.

Type	BET [m^2 g^{-1}]	Q_{irr} [mAh g^{-1}]	q_{irr} [mC cm^{-2}]
Black Acetylene	64	737	4.15
Carbon Nanofibers	36	624	6.24
Super-P	65	484	2.68
Graphite	13	143	3.96

Within this frame, XPS studies performed onto NMC-[179] and transition metal phosphate-based[33] electrodes suggested that the surface layer may be formed preferentially on the carbon particles and/or the polymeric binder, in solutions containing 1 M LiPF$_6$ dissolved in EC:DMC (1:1) and in EC:DEC (1:1)[33,179] (Figure 22). However, direct SECM measurements performed onto NMC electrodes cycled in 1 M LiPF$_6$ EC:DEC (1:1) probed an electronically conductive surface when a composite electrode made only of conductive carbon particles was cycled[65] (Figure 23).
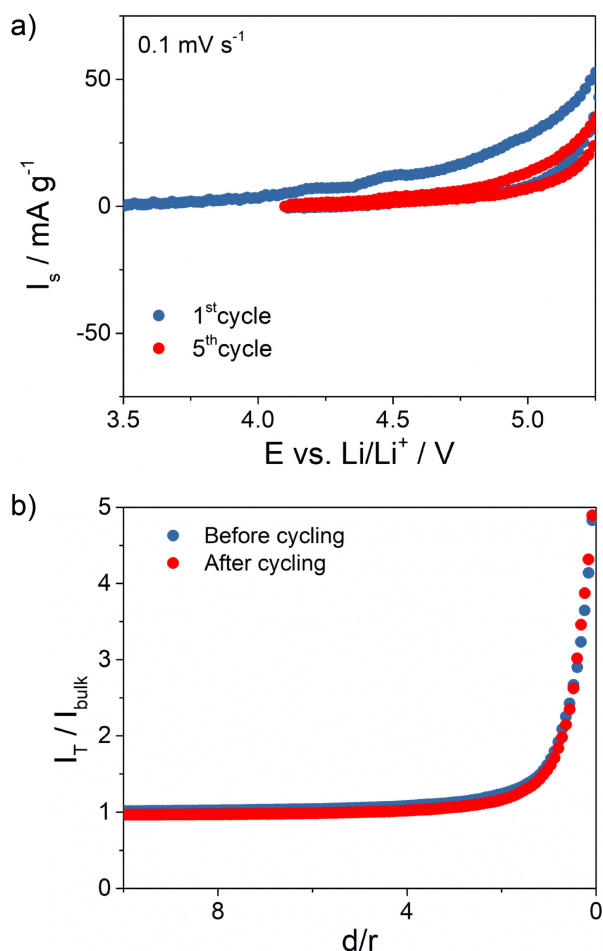
Thus, it remains not clear whether the formation of the surface layer on the conductive carbon additive and polymeric binder (if any) does not block the electron transfer because of it does not form homogeneously, it is too thin to prevent the electron tunnelling, or it is permeable to the electrolyte molecules.

4.4.2. Aluminium current collector.

Metallic aluminium is the preferred current collector in the positive electrode side within most of the organic-based Li-ion batteries thanks to its high conductivity, low weight, high stability at anodic potentials, and low cost.[36,65,186–188] However, a thin layer of Al$_2$O$_3$ is supposed to be present on the Al current collector surface, even after the polishing steps occurring under argon atmosphere. The formation of the aluminium oxide layer may occur spontaneously because of the presence of O$_2$ in the inert Ar atmosphere, even when the oxygen concentration is below 1 ppm.[189–190] On Al current collectors the formation of an electronically insulating surface layer is desired not only to prevent any further electrolyte decomposition, but also to avoid the corrosion of the metallic current collector during the battery operation.

Batteries & Supercaps

Reviews

doi.org/10.1002/batt.201900177

Chemistry
Europe
European Chemical
Societies Publishing

Figure 23. a) Cyclic voltammogram of a C65 based paste electrode in 1 M LiPF$_6$ EC : DEC (1 : 1 wt%).; b) z-Approach curves (r: radius of the tip: 12.5 mm; d: tip-to-sample distance) to the C65 surface before and after the cyclic voltammogram. Z approach curves recorded in 15 mM FcPF$_6$ 1 M LiPF$_6$ EC : DEC (1 : 1 wt%). Paste electrode held at OCP (4.1 V); applied tip potential: 3.0 V. Reprinted with permission from Ref. [65]. Copyright (2017) PCCP Owner Societies.

In situ FTIR, XPS, SEM and electrochemical studies performed in different solvents (such as PC, EC : DEC, EC : DMC, etc.),[36,65,186–188] showed that the passivation of the aluminium surface depends on the solvents and Li salts molecules present in solution, together with the surface roughness of the Al electrode.[36,187–188] Specifically, there is a change of composition (Figure 24) and of morphology (Figure 25) of the passivation layer on Al in dependence of the composition of the organic solution in which the current collector is cycled.

Moreover, when aluminium is in contact with LiPF$_6$ the thin passivation layer is more electronically insulating than in the case when Al is in contact with LiClO$_4$ containing electrolytes,[36,187] probably because of the presence of insulating AlF$_3$ and non-stoichiometric Al-O—F species.[186,188] SECM studies, performed onto a metallic Al electrode immersed in EC : DEC containing 1 M LiPF$_6$ or 1 M LiClO$_4$, further demonstrated the effect of the lithium salt on the passivation grade of the Al surface[65] (Figure 26).
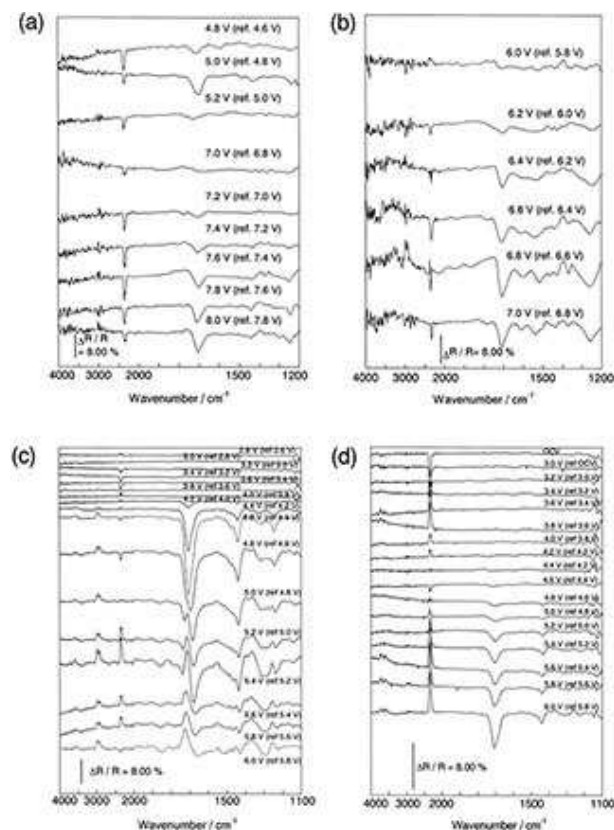
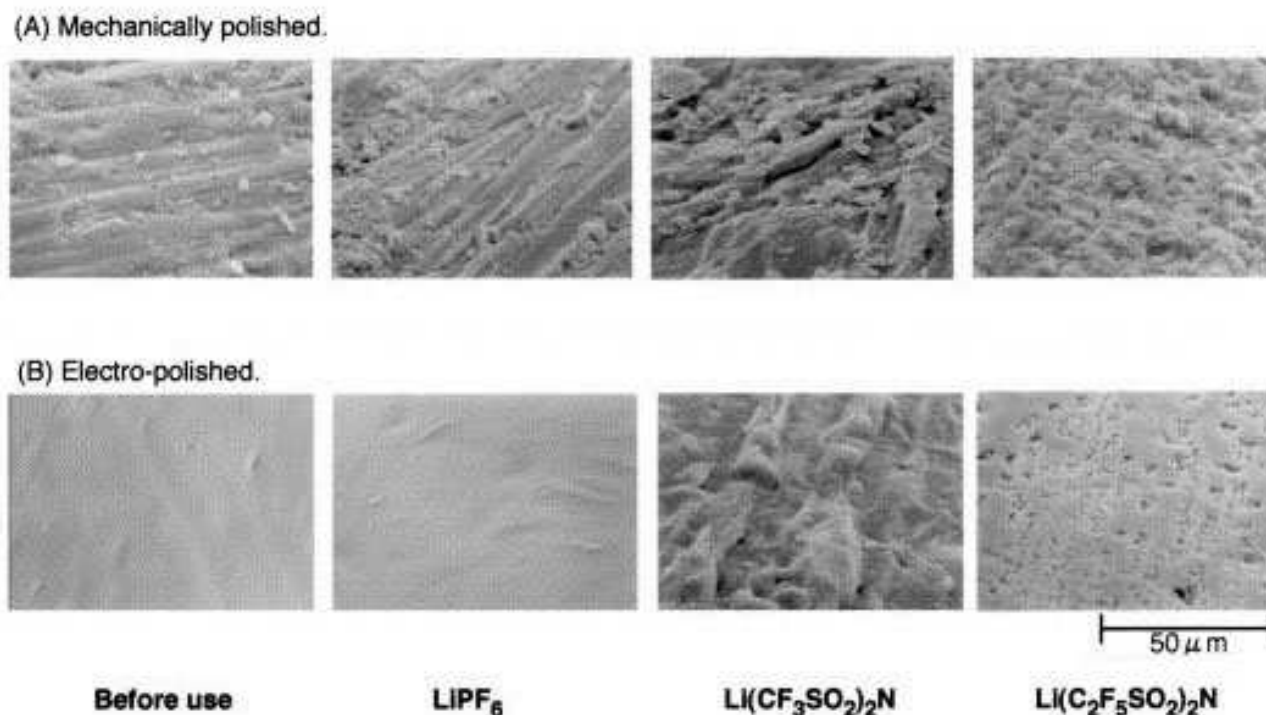**Figure 24.** In situ SNIFTIR spectra for propylene carbonate containing a) 1.0 mol dm^{-3} LiClO$_4$, b) 1.0 mol dm^{-3} LiPF$_6$, c) 1.0 mol dm^{-3} Li(CF$_3$SO$_2$)$_2$N, or d) 1.0 mol dm^{-3} Li(CF$_3$SO$_2$)(C$_4$F$_9$SO$_2$)N on the Al electrode. Reprinted with permission from Ref. [36]. Copyright (1999) Elsevier.

The reaction mechanism of the electrolyte irreversible oxidation on Al current collector is still unclear. It has been suggested that the oxidation of the electrolyte may depend on the stability of the Al surface film (which is dependent on the anionic species present in solution),[36] and it may proceed through the oxidation and successively decomposition of the anion onto the Al surface.[187]

5. Conclusions and Perspectives

Despite the critical importance of the nature and properties of the SEI formed onto the negative electrodes on the performance, cycle life and safety of a Li-ion battery, the analysis of such interphase is not trivial in terms of proper data acquisition and interpretation. This leads to contradicting literature on the composition, structure, electrochemical, chemical and mechanical properties, etc., of the SEI.

The situation is even more critical on the positive electrode since the surface layer, which is formed because of the irreversible oxidative decomposition of the electrolyte, is even harder to visualise and to study. Considering the fact that the challenges posed by electromobility require higher energy density Li-ion batteries, it is nowadays of tremendous importance to investigate and to better understand the nature and

Batteries & Supercaps

Reviews
doi.org/10.1002/batt.201900177

Chemistry Europe
European Chemical
Societies Publishing

Figure 25. SEM images of Al surface after the potential cycling in 1 mol dm^{-3} LiX/(EC + DMC). Reprinted with permission from Ref. [188]. Copyright (2002) Elsevier.

the role of the interphase formed onto high operating potential positive electrodes. The little and often contradictory knowledge that is currently available on such surface layer is related to the lower number of dedicated studies, in comparison to its counterpart at the negative electrode side, and to the lack of systematic testing of different electrolyte's components (solvents, salts, and additives).

One of the major difficulties in the analysis of the surface layers is that none of the analytical tools that are used for the interphase investigation is a stand-alone technique. The weak points of the analytical techniques are often ignored or overlooked during the interpretation and the analysis of the acquired data, thus producing misleading results and reports. Moreover, some important properties of the interphase (such as the electronic insulating character, just to name one) are often not directly measured, but rather indirectly inferred.

In order to gather a more comprehensive and solid knowledge of the interphases in Li-ion batteries, especially on the positive electrode side, it is therefore of vital importance to systematically study such surface layers through the hyphenation and the combination of several analytical tools. In this way, collecting broader and complementary information will lead to a clearer overview of the characteristics and the role of such interphases in a high energy Li-ion cell.

Moreover, when possible, *in situ* measurements are to be preferred over the *ex situ* ones, in order to avoid any alteration of the surface layers. On the other hand, when possible, *operando* measurements should be preferred over the *in situ*

ones, in order to better understand the wished property and its changes in dependence on the cycling and on the aging of the electrodes. If the chosen analytical technique does not allow the operation *operando* and/or *in situ*, the *ex situ* measurements must be performed with the careful attention that they require. In particular, the contact with air (even in traces) should be avoided in any moment in order to avoid any unwanted modification of the surface layer under analysis.

Also passive components should be taken into account, and a more detailed and dedicate analysis is necessary in order to understand their role in the irreversible oxidation of the electrolyte and in the formation of the surface layer at the positive electrodes.

In conclusion, despite the high complexity of the interphase formed onto the positive electrodes, a deeper understanding of such surface layers together with their formation and nature might contribute in enabling effective and stable SEI-like layers on the positive electrode side as well. This will allow developing lithium-ion batteries with higher energy densities, which will be greatly beneficial for future electromobility applications.

Acknowledgements
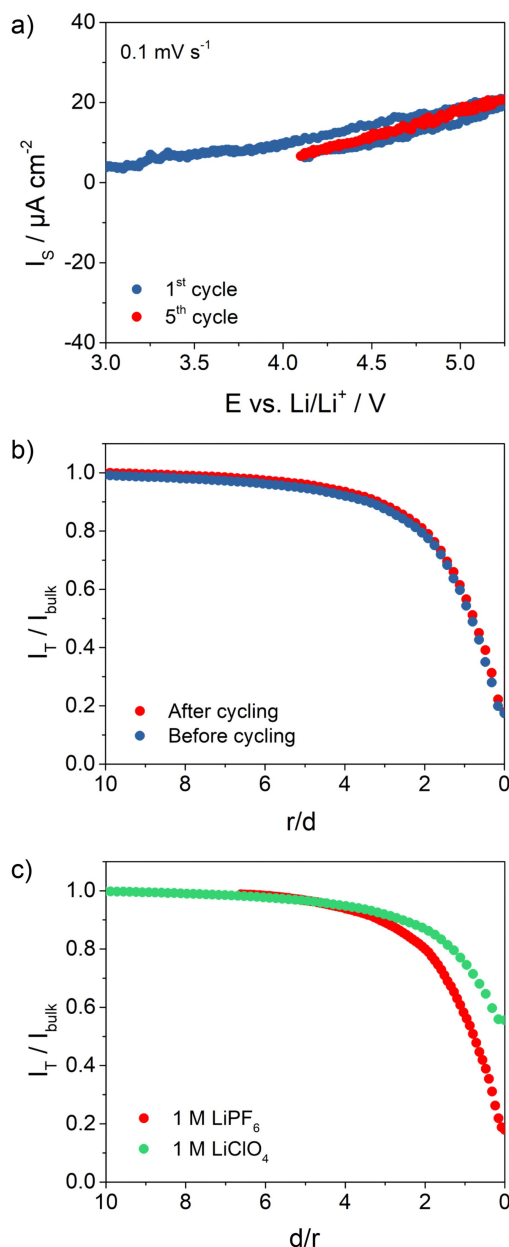
Figure 26. a) Cyclic voltammograms of the Al current collector cycled in 1 M LiPF$_6$ EC:DEC (1:1 wt%).; b) z-approach curves before and after the experiment. Al current collector held at OCP (4.1 V). c) z-Approach curves towards a fresh Al current collector cycled in two different solutions containing 1 M LiPF$_6$ and 1 M LiClO$_4$ EC:DEC (1:1 wt%), respectively. The Al current collector was held at OCP (3.2 V). Reprinted with permission from Ref. [65]. Copyright (2017) PCCP Owner Societies.

Conflict of Interest

The authors declare no conflict of interest.

Keywords: analytical techniques · cathodes · electrode-electrolyte interface · lithium-ion batteries · positive electrodes · solid-electrolyte interphase · surface layer · solid permeable interphase · cathode-electrolyte interphase

[1] A. Dushina, J. Stojadinovic, F. La Mantia, *Electrochim. Acta* **2015**, *167*, 262–267.
[2] J. Stojadinovic, A. Dushina, R. Trocoli, F. La Mantia, *ChemPlusChem* **2014**, *79*, 1507–1511.
[3] R. Fong, U. Vonsacken, J. R. Dahn, *J. Electrochem. Soc.* **1990**, *137*, 2009–2013.
[4] E. Peled, *J. Electrochem. Soc.* **1979**, *126*, 2047–2051.
[5] H. Buqa, R. I. R. Blyth, P. Golob, B. Evers, I. Schneider, M. V. S. Alvarez, F. Hofer, F. P. Netzer, M. G. Ramsey, M. Winter, J. O. Besenhard, *Ionics* **2000**, *6*, 172–179.
[6] P. Verma, P. Maire, P. Novak, *Electrochim. Acta* **2010**, *55*, 6332–6341.
[7] K. Xu, *Chem. Rev.* **2004**, *104*, 4303–4417.
[8] M. Arakawa, J. I. Yamaki, *J. Electroanal. Chem.* **1987**, *219*, 273–280.
[9] J. O. Besenhard, H. P. Fritz, *Angew. Chem. Int. Ed. Engl.* **1983**, *22*, 950–975.
[10] J. B. Goodenough, Y. Kim, *Chem. Mater.* **2010**, *22*, 587–603.
[11] J. O. Besenhard, M. Winter, J. Yang, W. Biberacher, *J. Power Sources* **1995**, *54*, 228–231.
[12] J. G. Thevenin, R. H. Muller, *J. Electrochem. Soc.* **1987**, *134*, 273–280.
[13] E. Peled, D. Golodnitsky, G. Ardel, *J. Electrochem. Soc.* **1997**, *144*, L208-L210.
[14] E. Peled, D. Golodnitsky, G. Ardel, V. Eshkenazy, *Electrochim. Acta* **1995**, *40*, 2197–2204.
[15] K. Kanamura, H. Tomura, S. Shiraishi, Z. I. Takehara, *J. Electrochem. Soc.* **1995**, *142*, 340–347.
[16] O. C. Harris, M. H. Tang, *J. Phys. Chem. C* **2018**, *122*, 20632–20641.
[17] K. Xu, *Chem. Rev.* **2014**, *114*, 11503–11618.
[18] M. Tang, S. D. Lu, J. Newman, *J. Electrochem. Soc.* **2012**, *159*, A1775-A1785.
[19] S. Kaymaksiz, M. Wachtler, M. Wohlfahrt-Mehrens, *J. Power Sources* **2015**, *273*, 123–127.
[20] T. Kranz, S. Kranz, V. Miß, J. Schepp, B. Roling, *J. Electrochem. Soc.* **2017**, *164*, A3777-A3784.
[21] M. Tang, J. Newman, *J. Electrochem. Soc.* **2011**, *158*, A530-A536.
[22] M. Winter, *Z. Phys. Chemie-Int. J. Res. Phys. Chem. Chem. Phys.* **2009**, *223*, 1395–1406.
[23] S. Krueger, R. Kloepsch, J. Li, S. Nowak, S. Passerini, M. Winter, *J. Electrochem. Soc.* **2013**, *160*, A542-A548.
[24] S. J. Rezvani, R. Gunnella, A. Witkowska, F. Mueller, M. Pasquali, F. Nobili, S. Passerini, A. Di Cicco, *ACS Appl. Mater. Interfaces* **2017**, *9*, 4570–4576.
[25] M. Winter, W. K. Appel, B. Evers, T. Hodal, K. C. Moller, I. Schneider, M. Wachtler, M. R. Wagner, G. H. Wrodnigg, J. O. Besenhard, *Mon. Chem.* **2001**, *132*, 473–486.
[26] M. Winter, J. O. Besenhard, M. E. Spahr, P. Novak, *Adv. Mater.* **1998**, *10*, 725–763.
[27] M. S. Whittingham, *Chem. Rev.* **2004**, *104*, 4271–4301.
[28] A. K. Padhi, K. S. Nanjundaswamy, J. B. Goodenough, *J. Electrochem. Soc.* **1997**, *144*, 1188–1194.
[29] M. Hirayama, H. Ido, K. Kim, W. Cho, K. Tamura, J. Mizuki, R. Kanno, *J. Am. Chem. Soc.* **2010**, *132*, 15268–15276.
[30] F. La Mantia, F. Rosciano, N. Tran, P. Novak, *J. Appl. Electrochem.* **2008**, *38*, 893–896.
[31] V. Blay, R. E. Galian, L. M. Muresan, D. Pankratov, P. Pinyou, G. Zampardi, *Adv. Sustainable Systems*, *n/a*, 1900145.
[32] K. Edstrom, T. Gustafsson, J. O. Thomas, *Electrochim. Acta* **2004**, *50*, 397–403.
[33] N. Membreno, K. Park, J. B. Goodenough, K. J. Stevenson, *Chem. Mater.* **2015**, *27*, 3332–3340.
[34] A. M. Andersson, D. P. Abraham, R. Haasch, S. MacLaren, J. Liu, K. Amine, *J. Electrochem. Soc.* **2002**, *149*, A1358–A1369.
[35] D. Aurbach, K. Gamolsky, B. Markovsky, Y. Gofer, U. Heider, R. Oesten, M. Schmidt, *J. Electrochem. Soc.* **2000**, *147*, 1322–1331.
[36] K. Kanamura, *J. Power Sources* **1999**, *81*, 123–129.
[37] T. Matsushita, K. Dokko, K. Kanamura, *J. Power Sources* **2005**, *146*, 360–364.
[38] S. Wasmus, W. Vielstich, *Electrochim. Acta* **1993**, *38*, 541–552.
[39] D. Guyomard, J. M. Tarascon, *J. Electrochem. Soc.* **1992**, *139*, 937–948.
[40] D. Guyomard, J. M. Tarascon, *J. Electrochem. Soc.* **1993**, *140*, 3071–3081.
[41] N. Liu, H. Li, Z. Wang, X. Huang, L. Chen, *Electrochem. Solid-State Lett.* **2006**, *9*, A328–A331.
[42] M. Borner, P. Niehoff, B. Vortmann, S. Nowak, M. Winter, F. M. Schappacher, *Energy Technol.* **2016**, *4*, 1631–1640.

Batteries & Supercaps

Reviews
doi.org/10.1002/batt.201900177

Chemistry
Europe

European Chemical
Societies Publishing

[43] D. Aurbach, B. Markovsky, G. Salitra, E. Markevich, Y. Talyossef, M. Koltypin, L. Nazar, B. Ellis, D. Kovacheva, *J. Power Sources* **2007**, *165*, 491–499.

[44] K. Kanamura, T. Umegaki, M. Ohashi, S. Toriyama, S. Shiraishi, Z. Takehara, *Electrochim. Acta* **2001**, *47*, 433–439.

[45] F. Croce, F. Nobili, A. Deptula, W. Lada, R. Tossici, A. D'Epifanio, B. Scrosati, R. Marassi, *Electrochem. Commun.* **1999**, *1*, 605–608.

[46] R. Imhof, P. Novak, *J. Electrochem. Soc.* **1999**, *146*, 1702–1706.

[47] B. Rasch, E. Cattaneo, P. Novak, W. Vielstich, *Electrochim. Acta* **1991**, *36*, 1397–1402.

[48] S.-i. Tobishima, T. Okada, *Electrochim. Acta* **1985**, *30*, 1715–1722.

[49] K. Xu, S. P. Ding, T. R. Jow, *J. Electrochem. Soc.* **1999**, *146*, 4172–4178.

[50] X. Zhang, R. Kostecki, T. J. Richardson, J. K. Pugh, P. N. Ross, *J. Electrochem. Soc.* **2001**, *148*, A1341–A1345.

[51] M. Winter, P. Novak, A. Monnier, *J. Electrochem. Soc.* **1998**, *145*, 428–436.

[52] P. Niehoff, S. Passerini, M. Winter, *Langmuir* **2013**, *29*, 5806–5816.

[53] D. Aurbach, *J. Power Sources* **2000**, *89*, 206–218.

[54] D. Aurbach, M. D. Levi, E. Levi, H. Teller, B. Markovsky, G. Salitra, U. Heider, L. Heider, *J. Electrochem. Soc.* **1998**, *145*, 3024–3034.

[55] S. Malmgren, K. Ciosek, M. Hahlin, T. Gustafsson, M. Gorgoi, H. Rensmo, K. Edstrom, *Electrochim. Acta* **2013**, *97*, 23–32.

[56] T. Eriksson, A. M. Andersson, A. G. Bishop, C. Gejke, T. Gustafsson, J. O. Thomas, *J. Electrochem. Soc.* **2002**, *149*, A69-A78.

[57] A. N. Mansour, *Surf. Sci. Spectra* **1994**, *3*, 279–286.

[58] A. Wursig, H. Buqa, M. Holzapfel, F. Krumeich, P. Novak, *Electrochem. Solid-State Lett.* **2005**, *8*, A34-A37.

[59] N. Dupré, J.-F. Martin, J. Oliveri, P. Soudan, D. Guyomard, A. Yamada, R. Kanno, *J. Electrochem. Soc.* **2009**, *156*, C180–C185.

[60] Z. Wang, Y. Sun, L. Chen, X. Huang, *J. Electrochem. Soc.* **2004**, *151*, A914.

[61] R. Dedryvère, D. Foix, S. Franger, S. Patoux, L. Daniel, D. Gonbeau, *J. Phys. Chem. C* **2010**, *114*, 10999–11008.

[62] S. Malmgren, H. Rensmo, T. Gustafsson, M. Gorgoi, K. Edstrom, in *Rechargeable Lithium-Ion Batteries, Vol. 25* (Eds.: M. Winter, D. H. Doughty, K. Zaghib, K. M. Abraham, Z. Ogumi, N. J. Dudney), Electrochemical Soc Inc, Pennington, **2010**, pp. 201–210.

[63] J. Demeaux, M. Caillon-Caravanier, H. Galiano, D. Lemordant, B. Claude-Montigny, *J. Electrochem. Soc.* **2012**, *159*, A1880-A1890.

[64] H. Duncan, D. Duguay, Y. Abu-Lebdeh, I. J. Davidson, *J. Electrochem. Soc.* **2011**, *158*, A537.

[65] G. Zampardi, R. Trocoli, W. Schuhmann, F. La Mantia, *Phys. Chem. Chem. Phys.* **2017**, *19*, 28381–28387.

[66] J. Conder, C. Marino, P. Novak, C. Villevieille, *J. Mater. Chem. A* **2018**, *6*, 3304–3327.

[67] S. F. Amalraj, D. Aurbach, *J. Solid State Electrochem.* **2011**, *15*, 877–890.

[68] P. Novak, J. C. Panitz, F. Joho, M. Lanz, R. Imhof, M. Coluccia, *J. Power Sources* **2000**, *90*, 52–58.

[69] S.-H. Lee, H.-G. You, K.-S. Han, J. Kim, I.-H. Jung, J.-H. Song, *J. Power Sources* **2014**, *247*, 307–313.

[70] K. Edstrom, M. Herstedt, D. P. Abraham, *J. Power Sources* **2006**, *153*, 380–384.

[71] S. S. Harilal, J. P. Allain, A. Hassanein, M. R. Hendricks, M. Nieto-Perez, *Appl. Surf. Sci.* **2009**, *255*, 8539–8543.

[72] B. Philippe, M. Hahlin, K. Edstrom, T. Gustafsson, H. Siegbahn, H. Rensmo, *J. Electrochem. Soc.* **2016**, *163*, A178–A191.

[73] K. Kanamura, H. Takezawa, S. Shiraishi, Z. Takehara, *J. Electrochem. Soc.* **1997**, *144*, 1900–1906.

[74] S. Perez-Villar, P. Lanz, H. Schneider, P. Novak, *Electrochim. Acta* **2013**, *106*, 506–515.

[75] F. Joho, P. Novak, *Electrochim. Acta* **2000**, *45*, 3589–3599.

[76] Y. Akita, M. Segawa, H. Munakata, K. Kanamura, *J. Power Sources* **2013**, *239*, 175–180.

[77] K. Hongyou, T. Hattori, Y. Nagai, T. Tanaka, H. Nii, K. Shoda, *J. Power Sources* **2013**, *243*, 72–77.

[78] Y. Ikezawa, T. Ariga, *Electrochim. Acta* **2007**, *52*, 2710–2715.

[79] C. Korepp, H. J. Santner, T. Fujii, M. Ue, J. O. Besenhard, K. C. Moller, M. Winter, *J. Power Sources* **2006**, *158*, 578–582.

[80] P. Novak, D. Goers, L. Hardwick, M. Holzapfel, W. Scheifele, J. Ufhiel, A. Wursig, *J. Power Sources* **2005**, *146*, 15–20.

[81] P. Lanz, P. Novak, *J. Electrochem. Soc.* **2014**, *161*, A1555–A1563.

[82] R. Imhof, P. Novak, *J. Electrochem. Soc.* **1998**, *145*, 1081–1087.

[83] F. La Mantia, P. Novak, *Electrochem. Solid-State Lett.* **2008**, *11*, A84-A87.

[84] P. Novak, F. Joho, R. Imhof, J. C. Panitz, O. Haas, *J. Power Sources* **1999**, *81*, 212–216.

[85] M. Heinrich, N. Wolff, N. Harting, V. Laue, F. Roder, S. Seitz, U. Krewer, *Batteries Supercaps* **2019**, *2*, 530–540.

[86] D. Koster, G. Q. Du, A. Battistel, F. La Mantia, *Electrochim. Acta* **2017**, *246*, 553–563.

[87] A. Battistel, G. Du, F. La Mantia, *Electroanalysis* **2016**, *28*, 2346–2353.

[88] A. M. Bond, R. J. Schwall, D. E. Smith, *J. Electroanal. Chem. Interfacial Electrochem.* **1977**, *85*, 231–247.

[89] S. Klink, D. Höche, F. La Mantia, W. Schuhmann, *J. Power Sources* **2013**, *240*, 273–280.

[90] S. Klink, E. Madej, E. Ventosa, A. Lindner, W. Schuhmann, F. La Mantia, *Electrochem. Commun.* **2012**, *22*, 120–123.

[91] M. Ender, A. Weber, E. Ivers-Tiffee, *J. Electrochem. Soc.* **2012**, *159*, A128-A136.

[92] A. Battistel, M. Fan, J. Stojadinovic, F. La Mantia, *Electrochim. Acta* **2014**, *135*, 133–138.

[93] F. La Mantia, C. D. Wessells, H. D. Deshazer, Y. Cui, *Electrochem. Commun.* **2013**, *31*, 141–144.

[94] J. P. Meyers, M. Doyle, R. M. Darling, J. Newman, *J. Electrochem. Soc.* **2000**, *147*, 2930–2940.

[95] F. La Mantia, J. Vetter, P. Novák, *Electrochim. Acta* **2008**, *53*, 4109–4121.

[96] P. Albertus, J. Christensen, J. Newman, *J. Electrochem. Soc.* **2009**, *156*, A606–A618.

[97] J. Newman, K. E. Thomas, H. Hafezi, D. R. Wheeler, *J. Power Sources* **2003**, *119*, 838–843.

[98] D. Alliata, R. Kotz, P. Novak, H. Siegenthaler, *Electrochem. Commun.* **2000**, *2*, 436–440.

[99] K. Edstrom, M. Herranen, *J. Electrochem. Soc.* **2000**, *147*, 3628–3632.

[100] Y. Domi, M. Ochida, S. Tsubouchi, H. Nakagawa, T. Yamanaka, T. Doi, T. Abe, Z. Ogumi, *J. Phys. Chem. C* **2011**, *115*, 25484–25489.

[101] G. Zampardi, S. Klink, V. Kuznetsov, T. Erichsen, A. Maljusch, F. La Mantia, W. Schuhmann, E. Ventosa, *ChemElectroChem* **2015**, *2*, 1607–1611.

[102] Q. P. McAllister, K. E. Strawhecker, C. R. Becker, C. A. Lundgren, *J. Power Sources* **2014**, *257*, 380–387.

[103] S. Q. Huang, S. W. Wang, G. H. Hu, L. Z. Cheong, C. Shen, *Appl. Surf. Sci.* **2018**, *441*, 265–271.

[104] J. Hwang, H. Jang, *J. Electrochem. Soc.* **2015**, *162*, A103-A107.

[105] V. Kuznetsov, A. H. Zinn, G. Zampardi, S. Borhani-Haghighi, F. La Mantia, A. Ludwig, W. Schuhmann, E. Ventosa, *ACS Appl. Mater. Interfaces* **2015**, *7*, 23554–23563.

[106] M. G. Verde, L. Baggetto, N. Balke, G. M. Veith, J. K. Seo, Z. Y. Wang, Y. S. Meng, *ACS Nano* **2016**, *10*, 4312–4321.

[107] S. Yang, B. G. Yan, T. Li, J. Zhu, L. Lu, K. Y. Zeng, *Phys. Chem. Chem. Phys.* **2015**, *17*, 22235–22242.

[108] X. J. Zhu, C. S. Ong, X. X. Xu, B. L. Hu, J. Shang, H. L. Yang, S. Katlakunta, Y. W. Liu, X. X. Chen, L. Pan, J. Ding, R. W. Li, *Sci. Rep.* **2013**, *3*, 8.

[109] W. T. Yao, F. Long, R. Shahbazian-Yassar, *ACS Appl. Mater. Interfaces* **2016**, *8*, 29391–29399.

[110] Y. Domi, T. Doi, T. Yamanaka, T. Abe, Z. Ogumi, *J. Electrochem. Soc.* **2013**, *160*, A678-A683.

[111] Y. Domi, M. Ochida, S. Tsubouchi, H. Nakagawa, T. Yamanaka, T. Doi, T. Abe, Z. Ogumia, *J. Electrochem. Soc.* **2012**, *159*, A1292-A1297.

[112] S. Tsubouchi, Y. Domi, T. Doi, M. Ochida, H. Nakagawa, T. Yamanaka, T. Abe, Z. Ogumi, *J. Electrochem. Soc.* **2013**, *160*, A575–A580.

[113] A. v. Cresce, S. M. Russell, D. R. Baker, K. J. Gaskell, K. Xu, *Nano Lett.* **2014**, *14*, 1405–1412.

[114] I. T. Lucas, E. Pollak, R. Kostecki, *Electrochem. Commun.* **2009**, *11*, 2157–2160.

[115] A. v. Cresce, S. M. Russell, D. R. Baker, K. J. Gaskell, K. Xu, *Nano Lett.* **2014**, *14*, 1405–1412.

[116] C. S. Han, S. H. R. Sanei, F. Alisafaei, *J. Polym. Eng.* **2016**, *36*, 103–111.

[117] D. Passeri, M. Rossi, E. Tamburri, M. L. Terranova, *Anal. Bioanal. Chem.* **2013**, *405*, 1463–1478.

[118] C. G. Zoski, *J. Electrochem. Soc.* **2016**, *163*, H3088–H3100.

[119] G. Zampardi, E. Ventosa, F. La Mantia, W. Schuhmann, *Chem. Commun.* **2013**, *49*, 9347–9349.

[120] H. Bulter, F. Peters, J. Schwenzel, G. Wittstock, *Angew. Chem. Int. Ed.* **2014**, *53*, 10531–10535; *Angew. Chem.* **2014**, *126*, 10699–10704.

[121] G. Zampardi, E. Ventosa, F. La Mantia, W. Schuhmann, *Electroanalysis* **2015**, *27*, 1017–1025.

[122] H. Bulter, F. Peters, G. Wittstock, *Energy Technol.* **2016**, *4*, 1486–1494.

[123] E. Ventosa, G. Zampardi, C. Flox, F. La Mantia, W. Schuhmann, J. R. Morante, *Chem. Commun.* **2015**, *51*, 14973–14976.

Batteries & Supercaps

Reviews
doi.org/10.1002/batt.201900177

Chemistry Europe
European Chemical
Societies Publishing

[124] E. Ventosa, E. Madej, G. Zampardi, B. Mei, P. Weide, H. Antoni, F. La Mantia, M. Muhler, W. Schuhmann, *ACS Appl. Mater. Interfaces* **2017**, *9*, 3123–3130.

[125] G. Zampardi, F. La Mantia, W. Schuhmann, *RSC Adv.* **2015**, *5*, 31166–31171.

[126] G. Zampardi, F. La Mantia, W. Schuhmann, *Electrochem. Commun.* **2015**, *58*, 1–5.

[127] C. A. Bridges, X. G. Sun, J. K. Zhao, M. P. Paranthaman, S. Dai, *J. Phys. Chem. C* **2012**, *116*, 7701–7711.

[128] T. M. Fears, M. Doucet, J. F. Browning, J. K. S. Baldwin, J. G. Winiarz, H. Kaiser, H. Taub, R. L. Sacci, G. M. Veith, *Phys. Chem. Chem. Phys.* **2016**, *18*, 13927–13940.

[129] J. E. Owejan, J. P. Owejan, S. C. DeCaluwe, J. A. Dura, *Chem. Mater.* **2012**, *24*, 2133–2140.

[130] H. Kawaura, M. Harada, Y. Kondo, H. Kondo, Y. Suganuma, N. Takahashi, J. Sugiyama, Y. Seno, N. L. Yamada, *ACS Appl. Mater. Interfaces* **2016**, *8*, 9540–9544.

[131] P. M. B. Piccoli, T. F. Koetzle, A. J. Schultz, *Comments Inorg. Chem.* **2007**, *28*, 3–38.

[132] I. T. Lucas, J. Syzdek, R. Kostecki, *Electrochem. Commun.* **2011**, *13*, 1271–1275.

[133] S. F. Lux, I. T. Lucas, E. Pollak, S. Passerini, M. Winter, R. Kostecki, *Electrochem. Commun.* **2012**, *14*, 47–50.

[134] M. A. McArthur, S. Trussler, J. R. Dahn, *J. Electrochem. Soc.* **2012**, *159*, A198-A207.

[135] K. Kwon, F. P. Kong, F. McLarnon, J. W. Evans, *J. Electrochem. Soc.* **2003**, *150*, A229-A233.

[136] N. A. Padilla, M. T. Rea, M. Foy, S. P. Upadhyay, K. A. Desrochers, T. Derus, K. A. Knapper, N. H. Hunter, S. Wood, D. A. Hinton, A. C. Cavell, A. G. Masias, R. H. Goldsmith, *ACS Sens.* **2017**, *2*, 903–908.

[137] Y. L. Qiao, Z. Zhou, Z. X. Chen, S. C. Du, Q. Cheng, H. W. Zhai, N. J. Fritz, Q. Du, Y. Yang, *Nano Energy* **2018**, *45*, 68–74.

[138] R. Baddour-Hadjean, J. P. Pereira-Ramos, *Chem. Rev.* **2010**, *110*, 1278–1319.

[139] A. Jarry, S. Gottis, Y. S. Yu, J. Roque-Rosell, C. Kim, J. Cabana, J. Kerr, R. Kostecki, *J. Am. Chem. Soc.* **2015**, *137*, 3533–3539.

[140] R. Kostecki, L. Norin, X. Y. Song, F. McLarnon, *J. Electrochem. Soc.* **2004**, *151*, A522-A526.

[141] N. S. Norberg, S. F. Lux, R. Kostecki, *Electrochem. Commun.* **2013**, *34*, 29–32.

[142] M. D. Levi, L. Daikhin, D. Aurbach, V. Presser, *Electrochem. Commun.* **2016**, *67*, 16–21.

[143] M. D. Levi, S. Sigalov, G. Salitra, D. Aurbach, J. Maier, *ChemPhysChem* **2011**, *12*, 854–862.

[144] M. D. Levi, S. Sigalov, G. Salitra, R. Elazari, D. Aurbach, L. Daikhin, V. Presser, *J. Phys. Chem. C* **2013**, *117*, 1247–1256.

[145] Y. G. Ryu, S. Lee, S. Mah, D. J. Lee, K. Kwon, S. Hwang, S. Doo, *J. Electrochem. Soc.* **2008**, *155*, A583–A589.

[146] V. Dargel, N. Shpigel, S. Sigalov, P. Nayak, M. D. Levis, L. Daikhin, D. Aurbach, *Nat. Commun.* **2017**, *8*, 8.

[147] L. Larush-Asraf, A. Biton, H. Teller, E. Zinigrad, D. Aurbach, *J. Power Sources* **2007**, *174*, 400–407.

[148] N. Serizawa, S. Seki, K. Takei, H. Miyashiro, K. Yoshida, K. Ueno, N. Tachikawa, K. Dokko, Y. Katayama, M. Watanabe, T. Miura, *J. Electrochem. Soc.* **2013**, *160*, A1529-A1533.

[149] J. T. Li, S. R. Chen, X. Y. Fan, L. Huang, S. G. Sun, *Langmuir* **2007**, *23*, 13174–13180.

[150] K. Kwon, J. W. Evans, *Electrochim. Acta* **2004**, *49*, 867–872.

[151] D. A. Buttry, M. D. Ward, *Chem. Rev.* **1992**, *92*, 1355–1379.

[152] L. Daikhin, M. Urbakh, *Langmuir* **1996**, *12*, 6354–6360.

[153] L. A. Theisen, S. J. Martin, A. R. Hillman, *Anal. Chem.* **2004**, *76*, 796–804.

[154] J. Yano, V. K. Yachandra, *Photosynth. Res.* **2009**, *102*, 241–254.

[155] C. Bressler, M. Chergui, *Chem. Rev.* **2004**, *104*, 1781–1812.

[156] D. Takamatsu, Y. Koyama, Y. Orikasa, S. Mori, T. Nakatsutsumi, T. Hirano, H. Tanida, H. Arai, Y. Uchimoto, Z. Ogumi, *Angew. Chem. Int. Ed.* **2012**, *51*, 11597–11601; *Angew. Chem.* **2012**, *124*, 11765–11769.

[157] P. Shearing, Y. Wu, S. J. Harris, N. Brandon, *The Electrochemical Society Interface* **2011**, *20*, 43–47.

[158] S. Y. Liu, L. D. Y. Wang, C. C. Zhang, B. B. Chu, C. P. Wang, T. Huang, A. S. Yu, *J. Power Sources* **2019**, *438*, 8.

[159] H. Kawaura, D. Takamatsu, S. Mori, Y. Orikasa, H. Sugaya, H. Murayama, K. Nakanishi, H. Tanida, Y. Koyama, H. Arai, Y. Uchimoto, Z. Ogumi, *J. Power Sources* **2014**, *245*, 816–821.

[160] J. Wandt, A. Freiberg, R. Thomas, Y. Gorlin, A. Siebel, R. Jung, H. A. Gasteiger, M. Tromp, *J. Mater. Chem. A* **2016**, *4*, 18300–18305.

[161] S. J. Rezvani, R. Ciambezi, R. Gunnella, M. Minicucci, M. A. Munoz, F. Nobili, M. Pasqualini, S. Passerini, C. Schreiner, A. Trapananti, A. Witkowska, A. Di Cicco, *J. Phys. Chem. C* **2016**, *120*, 4287–4295.

[162] H. Ota, T. Akai, H. Namita, S. Yamaguchi, M. Nomura, *J. Power Sources* **2003**, *119*, 567–571.

[163] P. Barpanda, D. Dwibedi, S. Ghosh, Y. Kee, S. Okada, *Ionics* **2015**, *21*, 1801–1812.

[164] H. N. Girish, G. Q. Shao, *RSC Adv.* **2015**, *5*, 98666–98686.

[165] G. Rousse, J. M. Tarascon, *Chem. Mater.* **2014**, *26*, 394–406.

[166] B. Aktekin, M. J. Lacey, T. Nordh, R. Younesi, C. Tengstedt, W. Zipprich, D. Brandell, K. Edstrom, *J. Phys. Chem. C* **2018**, *122*, 11234–11248.

[167] H. Duncan, Y. Abu-Lebdeh, I. J. Davidson, *J. Electrochem. Soc.* **2010**, *157*, A528–A535.

[168] L. Yang, B. Ravdel, B. L. Lucht, *Electrochem. Solid-State Lett.* **2010**, *13*, A95–A97.

[169] K. J. Carroll, M.-C. Yang, G. M. Veith, N. J. Dudney, Y. S. Meng, *Electrochem. Solid-State Lett.* **2012**, *15*, A72.

[170] M. Matsui, K. Dokko, K. Kanamura, *J. Electrochem. Soc.* **2010**, *157*, A121–A129.

[171] Y. Talyosef, B. Markovsky, R. Lavi, G. Salitra, D. Aurbach, D. Kovacheva, M. Gorova, E. Zhecheva, R. Stoyanova, *J. Electrochem. Soc.* **2007**, *154*, A682–A691.

[172] T. J. Lee, H. S. Kim, H. S. Hwang, J. Soon, J. Jung, J. H. Ryu, S. M. Oh, *J. Electrochem. Soc.* **2018**, *165*, A575–A583.

[173] K. M. Shaju, P. G. Bruce, *Adv. Mater.* **2006**, *18*, 2330–2334.

[174] F. La Mantia, F. Rosciano, N. Tran, P. Novak, *J. Electrochem. Soc.* **2009**, *156*, A823–A827.

[175] E. J. Berg, C. Villevieille, D. Streich, S. Trabesinger, P. Novák, *J. Electrochem. Soc.* **2015**, *162*, A2468–A2475.

[176] E. Bjorklund, D. Brandell, M. Hahlin, K. Edstrom, R. Younesi, *J. Electrochem. Soc.* **2017**, *164*, A3054–A3059.

[177] D. J. Li, H. Li, D. Danilov, L. Gao, J. Zhou, R. A. Eichel, Y. Yang, P. H. L. Notten, *J. Power Sources* **2018**, *396*, 444–452.

[178] A. Maheshwari, M. Heck, M. Santarelli, *Electrochim. Acta* **2018**, *273*, 335–348.

[179] P. Niehoff, M. Winter, *Langmuir* **2013**, *29*, 15813–15821.

[180] D. J. Xiong, L. D. Ellis, J. Li, H. Y. Li, T. Hynes, J. P. Allen, J. Xia, D. S. Hall, I. G. Hill, J. R. Dahn, *J. Electrochem. Soc.* **2017**, *164*, A3025-A3037.

[181] C. F. Petersburg, Z. Li, N. A. Chernova, M. S. Whittingham, F. M. Alamgir, *J. Mater. Chem.* **2012**, *22*, 19993–20000.

[182] L. Simonin, J. F. Colin, V. Ranieri, E. Canevet, J. F. Martin, C. Bourbon, C. Baehtz, P. Strobel, L. Daniel, S. Patoux, *J. Mater. Chem.* **2012**, *22*, 11316–11322.

[183] T. Hayashi, J. Okada, E. Toda, R. Kuzuo, N. Oshimura, N. Kuwata, J. Kawamura, *J. Electrochem. Soc.* **2014**, *161*, A1007–A1011.

[184] H. Lyu, Y. C. Li, C. J. Jafta, C. A. Bridges, H. M. Meyer, A. Borisevich, M. P. Paranthaman, S. Dai, X. G. Sun, *J. Power Sources* **2019**, *412*, 527–535.

[185] F. La Mantia, R. A. Huggins, Y. Cui, *J. Appl. Electrochem.* **2013**, *43*, 1–7.

[186] C. Iwakura, Y. Fukumoto, H. Inoue, S. Ohashi, S. Kobayashi, H. Tada, M. Abe, *J. Power Sources* **1997**, *68*, 301–303.

[187] K. Kanamura, T. Okagawa, Z.-i. Takehara, *J. Power Sources* **1995**, *57*, 119–123.

[188] M. Morita, T. Shibata, N. Yoshimoto, M. Ishikawa, *Electrochim. Acta* **2002**, *47*, 2787–2793.

[189] N. Cabrera, N. F. Mott, *Rep. Prog. Phys.* **1949**, *12*, 163–184.

[190] C. Gong, D. Ruzmetov, A. Pearse, D. Ma, J. N. Munday, G. Rubloff, A. A. Talin, M. S. Leite, *ACS Appl. Mater. Interfaces* **2015**, *7*, 26007–26011.